

THE ORIGIN AND EVOLUTION OF HALO BIAS IN LINEAR AND NON-LINEAR REGIMES

ANDREY V. KRAVTSOV AND ANATOLY A. KLYPIN

Astronomy Department, New Mexico State University, Box 30001, Dept. 4500, Las Cruces, NM 88003-0001

Astrophysical Journal, submitted

ABSTRACT

We present results from a study of bias and its evolution for galaxy-size halos in a large, high-resolution simulation of a low-density, cold dark matter model with a cosmological constant. We consider the evolution of bias estimated using three different statistics: two-point correlation function b_ξ , power spectrum b_P , and a direct correlation of smoothed halo and matter overdensity fields b_δ . We present accurate estimates of the evolution of the matter power spectrum probed deep into the stable clustering regime ($k \sim [0.1-200]h \text{ Mpc}^{-1}$ at $z = 0$) and find that its shape and evolution can be well described, with only a minor modification, by the fitting formula of Peacock & Dodds (1996). The halo power spectrum evolves much slower than the power spectrum of matter and has a different shape which indicates that the bias is time- and scale-dependent. At $z = 0$, the halo power spectrum is anti-biased ($b_P < 1$) with respect to the matter power spectrum at wavenumbers $k \sim [0.15-30]h \text{ Mpc}^{-1}$, and provides an excellent match to the power spectrum of the APM galaxies at all probed k . In particular, both the halo and matter power spectra show an inflection at $k \approx 0.15h \text{ Mpc}^{-1}$, which corresponds to the present-day scale of non-linearity and nicely matches the inflection observed in the APM power spectrum. We complement the power spectrum analysis with a direct estimate of bias using smoothed halo and matter overdensity fields and show that the evolution observed in the simulation in linear and mildly non-linear regimes can be well described by the analytical model of Mo & White (1996), *if* the distinction between formation redshift of halos and observation epoch is introduced into the model. We present arguments and evidence that at higher overdensities, the evolution of bias is significantly affected by dynamical friction and tidal stripping operating on the satellite halos in high-density regions of clusters and groups; we attribute the strong anti-bias observed in the halo correlation function and power spectrum to these effects.

The results of this study show that despite the apparent complexity, the origin and evolution of bias can be understood in terms of the processes that drive the formation and evolution of dark matter halos. These processes conspire to produce a halo distribution quite different from the overall distribution of matter, yet remarkably similar to the observed distribution of galaxies.

Subject headings: cosmology: theory – large-scale structure of universe – methods: numerical

1. INTRODUCTION

The distribution of galaxies may, in general, be biased with respect to the overall matter distribution. Therefore, the galaxy density field can be used as a probe of matter distribution only if we fully understand how the galaxy distribution relates to the distribution of matter. Understanding this relationship, the bias, and its evolution are of primary importance for the interpretation of the ever increasing amount of high-quality galaxy clustering data at low and high redshifts. Although the problem of bias has been studied extensively during the last decade (e.g., Kaiser 1984; Davis et al. 1985; Bardeen et al. 1986; Dekel & Silk 1986; Cole & Kaiser 1989; Babul & White 1991), new data on galaxy clustering at high redshifts (e.g., at $z \lesssim 1$, Le Fèvre et al. 1996; Shepherd et al. 1997; Carlberg et al. 1997; Connolly et al. 1998; Postman et al. 1998; Carlberg et al. 1998; and, at $z \sim 3$, Steidel et al. 1998; Giavalisco et al. 1998; Adelberger et al. 1998) and the anticipation of upcoming accurate measurements of galaxy clustering at $z \approx 0$ from large redshift surveys (e.g., Tegmark et al. 1998, and references therein) have recently generated substantial theoretical progress in modelling of galaxy clustering and bias.

In hierarchical structure formation models, galaxies are

assumed to form inside dark matter (DM) halos via the energy dissipation by baryons (see Somerville & Primack 1998 for a recent review). Mo & White (1996) showed how bias of dark matter can be predicted analytically in the framework of the extended Press-Schechter theory (Bond et al. 1991; Bower 1991; Lacey & Cole 1993; see §2). This analytical model is rapidly gaining popularity in theoretical analyses (see, e.g., recent studies by Kauffman, Nusser & Steinmetz 1997, Moscardini et al. 1998, and Baugh et al. 1998) which requires it to be tested and its capabilities and limitations evaluated. The model has been tested against numerical simulations by Mo, Jing & White (1996), CateLAN, Matarrese & Porciani (1998), Jing (1998), and Porciani, CateLAN & Lacey (1998), and we present additional tests in this paper. More elaborate analytical models have been developed by CateLAN et al. (1998ab), Porciani et al. (1998a), and Sheth & Lemson (1998).

The effects of non-linearity of the bias on the observable statistics have been studied by Fry & Gaztañaga (1993), Coles (1993), and Mann, Peacock & Heavens (1997) using heuristic models of local non-linear bias. Recently, Coles (1993) and Dekel & Lahav (1998) have developed a formalism for studies of galaxy biasing that allows one to account explicitly for the non-linearity and stochasticity of the

bias. They have also analyzed the effects of non-linearity and stochasticity on results of some of the observational analyses. Sherrer & Weinberg (1998) have analyzed effects of stochasticity of the local bias on the correlation function and power spectrum and concluded that stochasticity should not affect the shape of these statistics in the linear regime (or, in other words, that in linear regime the bias should be linear). Most recently, Narayanan, Berlind & Weinberg (1998) studied effects of non-linearity, stochasticity, and non-locality of the bias using heuristic models applied to large N -body simulations. From the observational perspective, Pen (1998) showed how the stochasticity of the galaxy bias can be tested and measured using redshift-space distortions, and Tegmark & Bromley (1998) presented evidence that present-day galaxy bias is non-linear and stochastic based on analysis of galaxy clustering in the Las Campanas Redshift Survey.

The evolution of bias in the linear regime has been recently analyzed by Tegmark & Peebles (1998), who generalized the results of Fry (1996) for the case of stochastic bias in an arbitrary cosmology. Taruya, Koyama & Soda (1998) and Taruya & Soda (1998) used perturbative analysis to extend the linear analysis of bias evolution into the weakly non-linear regime. Evolution of halo clustering and bias in the non-linear regime, has been analyzed in several recent numerical studies employing dissipationless simulations (e.g., Brainerd & Villumsen 1994; Bagla 1998; Colín et al. 1998; Ma 1999), simulations that include both dissipationless dark matter and dissipative baryonic components (e.g., Katz, Hernquist & Weinberg 1998; Blanton et al. 1998; Cen & Ostriker 1998; Jenkins et al. 1998b), and “hybrid” studies in which dissipationless simulations are complemented with a semi-analytical model of galaxy formation (Roukema et al. 1997; Kauffman et al. 1998ab; Diaferio et al. 1998; Benson et al. 1998; Baugh et al. 1998; Kolatt et al. 1998). All of these studies, though very diverse in their methods, qualitatively agree on one important result: the galaxy bias is expected to be non-linear, to depend on the properties of the DM halos and the galaxies they host, and to be a (generally non-monotonic) function of cosmic time.

In this paper we present results of a detailed analysis of halo clustering evolution in a large high-resolution dissipationless simulation of a representative and fairly successful variant of the cold dark matter (CDM) models: the low-density spatially flat CDM model with the cosmological constant (Λ CDM). The primary goal of this analysis is to identify and study the main processes that drive the evolution of halo bias in linear and non-linear regimes. Understanding what causes the bias and particular features of its evolution (notably, the anti-bias at late stages of evolution in some of the models) is crucial for the interpretation of current observational and theoretical results. We focus therefore on the interpretation of general features of bias evolution observed in our simulations and in studies done by other authors. The main novel feature of this study is inclusion of satellite halos located inside virial radii of more massive isolated halos in the halo catalogs; we refer reader to Colín et al. (1998) for a more detailed description of our approach.

The approach that we have adopted in this project is to consider bias estimated using three different statistics: two-point correlation function $\xi(r)$, power spectrum $P(k)$

(Peebles 1980), and direct comparison of the smoothed halo and matter overdensity (δ) fields:

$$b_\xi(r) \equiv \sqrt{\xi_h(r)/\xi_m(r)}, \quad (1)$$

$$b_P(k) \equiv \sqrt{P_h(k)/P_m(k)}, \quad (2)$$

$$b_\delta \equiv \delta_h^R/\delta_m^R, \quad (3)$$

where quantities with subscripts h and m correspond to statistics of the halo and matter distributions, respectively, and superscript R indicates the density fields smoothed on a scale R . The three estimates of bias given above are, of course, related. In the special case of deterministic local linear bias: $b_\xi = b_P = b_\delta$. Nevertheless, in the general case of stochastic non-linear bias, these estimates are complementary to each other and we have chosen to consider all three of them to illustrate the manifestations and properties of the bias. All three functions, b_ξ , b_P , and b_δ , may depend on a number of (both local and non-local) parameters; the most important point to notice, however, is that they are different functions of their parameters, and we use the subscripts to indicate this explicitly. For example, b_ξ and b_P have different scale-dependence because $\xi(r)$ and $P(k)$ are related via the Fourier transform, $\xi(r) \propto \int P(k)e^{i\mathbf{k}\cdot\mathbf{r}}d^3k$, which gives:

$$b_\xi(r) = \frac{\int b_P(k)P_m(k)e^{i\mathbf{k}\cdot\mathbf{r}}d^3k}{\int P_m(k)e^{i\mathbf{k}\cdot\mathbf{r}}d^3k}. \quad (4)$$

The bias $b_\xi(r)$ that is scale-dependent in a narrow range of r will be scale-dependent in a wide range of k (see Coles 1993 for a more detailed discussion). We will show below that the anti-bias required at small r for the Λ CDM model to be consistent with the $z = 0$ galaxy correlation function, is also perfectly consistent with $b_P(k) < 1$ at small wavenumbers (down to $k \sim 0.2h \text{ Mpc}^{-1}$) required for the model to be consistent with the galaxy power spectrum (Gaztañaga & Baugh 1998; Hoyle et al. 1998).

The paper is organized as follows. In §2, we give a brief account of analytical model of the bias developed by Mo & White (1996) and how the epochs of halo formation and observation can be separated in this model (e.g., Moscardini et al. 1998; Catelan et al. 1998a). In §3 and §4 we describe the numerical simulation and halo identification and selection algorithms used in our analysis. We complement the analysis of the evolution of the halo two-point correlation function based on this simulation and presented in Colín et al. (1998) with the analysis of the evolution of the halo power spectrum and bias b_P in §5.1. In §5.2 and §5.3 we present the analysis of the evolution of b_δ , estimated using smoothed halo and matter density fields at different epochs, and identify the processes that drive this evolution. We discuss the results in §6 and summarize our conclusions and arguments in §7.

2. ANALYTICAL MODEL OF BIAS

An overdensity field $\delta(\mathbf{x}) \equiv [\rho(\mathbf{x}) - \bar{\rho}]/\bar{\rho}$ can be quantified in terms of its power spectrum $P(k) = \langle |\delta_{\mathbf{k}}|^2 \rangle$, where $\delta_{\mathbf{k}}$ is the Fourier transform of $\delta(\mathbf{x})$. Similarly, if the overdensity field is smoothed on scale R with a spherically symmetric filter $W(r, R)$, the smoothed field can be characterized by its variance

$$\sigma^2(R) = \langle [\delta(\mathbf{x}, R)]^2 \rangle = \frac{1}{(2\pi)^3} \int P(k)\hat{W}(R)^2 d^3k, \quad (5)$$

where \hat{W} is the Fourier transform of the window function. In the following and throughout the paper we use the *real space top-hat* filter: $W(r, R) = (4\pi R^3/3)^{-1}\Theta(R-r)$, where $\Theta(R-r)$ is the step function. For this filter the scale R can be interchanged with the mass contained within radius R : $M = (4\pi/3)\bar{\rho}R^3$, where $\bar{\rho}$ is the mean density of the universe. The standard Press-Schechter model (PS; Press & Schechter 1974) assumes that any region of initial comoving size R (or mass M) becomes a part of a virialized halo by redshift z_f , if its overdensity extrapolated linearly to the present epoch is greater than $\delta_c/D_+(z_f)$, where $D_+(z)$ is the linear growth factor (e.g., Peebles 1980) normalized to unity at the present epoch. The value of δ_c is motivated by the top-hat collapse model; we use $\delta_c = 1.69$ throughout this work. If the initial overdensity field is gaussian, the PS model leads to the following expression for the number density of collapsed halos of mass M at redshift z :

$$n(M, z, z_f)dM = \frac{1}{\sqrt{2\pi}} \frac{\bar{\rho}}{M} \frac{\delta_c(z, z_f)}{\sigma^3(M, z)} \left| \frac{d\sigma^2(M, z)}{dM} \right| \times \exp \left[-\frac{\delta_c(z, z_f)^2}{2\sigma^2(M, z)} \right] dM, \quad (6)$$

where $\delta_c(z, z_f) \equiv \delta_c D_+(z)/D_+(z_f)$ and $\sigma(M, z)$ is the variance of the initial density field smoothed on scale M and extrapolated linearly to the epoch z . For the reasons that will be discussed below, we follow Catelan et al. (1998a) in distinguishing the epoch z_f from the ‘‘observation’’ epoch z ($z < z_f$). The z_f - and z -dependencies are shown explicitly in the above expression for the mass function. Note, however, that $n(M, z, z_f)$ does not change with z : for a given power spectrum, the mass function depends only on halo mass M and z_f . Equation (6) translates into the commonly used form if we assume $z_f = z$.

In the seminal paper, Mo & White (1996; hereafter MW) showed how the extended Press-Schechter formalism (EPS; Bond et al. 1991; Bower 1991; Lacey & Cole 1993) can be used to derive the analytical expression for the bias of DM halos. The EPS can be used to derive the expression for the *conditional mass function* of halos (Bond et al. 1991). Namely, the number density of halos of mass M that collapse at epoch $z_f < z$ in a region of initial Lagrangian radius R_0 (mass M_0) and the initial overdensity in the growing mode extrapolated linearly to the present δ_0 ($\delta_0(z) = \delta_0 D_+(z)$) is given by

$$n(M, z, z_f|M_0, \delta_0)dM = \frac{1}{\sqrt{2\pi}} \frac{\bar{\rho}}{M} \frac{\delta_c - \delta_0}{[\sigma^2 - \sigma_0^2]^{3/2}} \left| \frac{d\sigma^2}{dM} \right| \times \exp \left\{ -\frac{[\delta_c - \delta_0]^2}{2[\sigma^2 - \sigma_0^2]} \right\} dM, \quad (7)$$

where $\delta_c \equiv \delta_c(z, z_f)$, $\delta_0 = \delta_0(z)$, $\sigma^2 \equiv \sigma^2(M, z)$, and $\sigma_0^2 \equiv \sigma^2(M_0, z)$, as defined above. The average overdensity of halos of mass M in spheres of overdensity δ_0 and radius R_0 at epoch z , $\delta_h(M, z|R_0, \delta_0)$, can be obtained by dividing number densities given by eqs. (7) and (6) and subtracting unity. The halo bias is then defined as $b \equiv \delta_h/\delta_0$. So far, the bias is defined in terms of the Lagrangian radius and linearly extrapolated overdensity. For practical purposes, however, we need the expression for bias in spheres of observed radius R and (generally non-linear) overdensity δ . MW use a spherical collapse model to relate (R_0, δ_0) to

(R, δ) : $R_0^3 = (1 + \delta)R^3$ and δ_0 are calculated for given R , R_0 , and δ using the equations of spherical collapse. Having made the translation from (R, δ) to (R_0, δ_0) , we can calculate the average overdensity of DM halos in spheres of the observed radius R and overdensity δ as

$$\delta_h(M, z, z_f|R, \delta) = (1 + \delta) \frac{n(M, z, z_f|R_0, \delta_0)}{n(M, z, z_f)} - 1, \quad (8)$$

$$b_{NL}(M, z, z_f, \delta) \equiv \delta_h(M, z, z_f|R, \delta)/\delta, \quad (9)$$

where b_{NL} is the halo bias. Note that in general b_{NL} depends on the overdensity of matter δ and is therefore non-linear. The quantities (R, δ) and (R_0, δ_0) in eq. (8) are related by the spherical collapse model. In the limit of linear overdensities and large scales, $\delta_0(z) \ll \delta_c(z, z_f)$ and $M_0 \gg M$, the bias is given by

$$b_L(M, z, z_f) = 1 + \frac{\nu^2 - 1}{\delta_c(z, z_f)}, \quad (10)$$

where $\nu \equiv \delta_c(z, z_f)/\sigma(M, z)$. Eq. (10) shows that in this regime the bias is linear (does not depend on δ). Note that the bias of halos with a range of masses $[M_{min}, M_{max}]$ should be computed as a mass function weighted average

$$b(z, z_f) = \bar{n}^{-1}(z, z_f) \int_{M_{min}}^{M_{max}} b(M, z, z_f) n(M, z, z_f) dM, \quad (11)$$

where $\bar{n}(z, z_f) = \int_{M_{min}}^{M_{max}} n(M, z, z_f) dM$ and $n(M, z, z_f)$ is given by eq. (6).

We use eqs. (8)-(11) to calculate the bias predicted by this analytical model. The linear overdensity δ_0 is calculated for given δ , R , and $R_0 = (1 + \delta)^{1/3}R$ using the equations of the spherical collapse model appropriate for our Λ CDM cosmology (e.g., Lahav et al. 1991; Eke et al. 1996). The resulting function $\delta_0(\delta)$ is well described by the fitting formula given by MW (eq.[18] in their paper), except for $\delta \sim 20 - 30$, where deviations reach $\approx 5 - 10\%$.

3. NUMERICAL SIMULATION

We have chosen to study the evolution of the halo bias in a representative variant of the CDM-type models: the low matter density, flat, CDM model with cosmological constant (Λ CDM): $\Omega_0 = 1 - \Omega_\Lambda = 0.3$, $h = 0.7$, where Ω_0 and Ω_Λ are present-day matter and vacuum densities, and h is the dimensionless Hubble constant defined as $H_0 = 100h$ km/s/Mpc. This model is arguably the most successful model in matching a variety of existing data. Observations of galaxy cluster evolution (Eke et al. 1996), baryon fraction in clusters (Evrard 1997), and high-redshift supernovae (e.g., Perlmutter et al. 1998) strongly favor the value of matter density $\Omega_0 \approx 0.3$, while various observational measurements of the Hubble constant (e.g., Falco et al. 1997; Salaris & Cassisi 1998; Madore et al. 1998) tend to converge on the values of $h \approx 0.6 - 0.7$. We use a normalization of the spectrum of fluctuations that is consistent with both observed cluster abundances (Eke et al. 1996) and the 4-year COBE data (e.g., Bunn & White 1997): $\sigma_8 = 1$, where σ_8 is the rms fluctuation in spheres of $8h^{-1}$ Mpc comoving radius.

The numerical simulation of the Λ CDM model followed the evolution of $256^3 \approx 1.67 \times 10^7$ particles in a periodic $60h^{-1}$ Mpc box. The particle mass is thus $\approx 1.1 \times 10^9 h^{-1} M_\odot$. The simulation was run using Adaptive Refinement Tree N -body code (ART; Kravtsov, Klypin & Khokhlov 1997). The ART code reaches high force resolution by refining all high-density regions with an automated refinement algorithm. The refinements are recursive: the refined regions can also be refined, each subsequent refinement having half of the previous level’s cell size. This creates an hierarchy of refinement meshes of different resolution covering regions of interest. The criterion for refinement is *local overdensity* of particles: in the simulation presented in this paper the code refined an individual cell only if the density of particles (smoothed with the cloud-in-cell scheme; Hockney & Eastwood 1981) was higher than $n_{th} = 5$ particles. Therefore, *all* regions with overdensity higher than $\delta = n_{th} 2^{3L}/\bar{n}$, where \bar{n} is the average number density of particles in the cube, were refined to the refinement level L . For the simulation presented here, \bar{n} is 1/8. The peak formal dynamic range reached by the code on the highest refinement level is 32,768, which corresponds to the smallest grid cell of $1.83h^{-1}$ kpc; the actual force resolution is approximately a factor of two lower (see Kravtsov et al. 1997). The simulation that we analyze here has been used in Colín et al. (1998), and we refer the reader to this paper for further numerical details.

4. HALO IDENTIFICATION AND SELECTION

Identification of DM halos in the very high-density environments (e.g., inside groups and clusters) is a challenging problem. The goal of this study is to investigate the halo bias at both low and high matter overdensities, and we therefore need to identify both isolated halos and satellite halos orbiting within the virial radii of larger systems. The problems associated with halo identification within high-density regions are discussed in Klypin et al. (1999; KGKK). In this study we use a halo finding algorithm called Bound Density Maxima (BDM). The main idea of the BDM algorithm is to find positions of local maxima in the density field smoothed at a certain scale and to apply physically motivated criteria to test whether the identified site corresponds to a gravitationally bound halo. The detailed description of the algorithm is given in KGKK and Colín et al. (1998). The publicly available version of the BDM algorithm used here is described in Klypin & Holtzman (1997). The halo catalogs used in the present study were constructed using numerical parameters given in Colín et al. (1998).

To construct a halo catalog, we have to define selection criteria based on particular halo properties. Halo mass is usually used to define halo catalogs (e.g., a catalog can be constructed by selecting all halos in a given mass range). However, the mass and radius are very poorly defined for the satellite halos due to tidal stripping which alters a halo’s mass and physical extent (see KGKK). Therefore, we will use maximum circular velocity V_{max} as a proxy for the halo mass. This allows us to avoid complications related to the mass and radius determination for satellite halos. Moreover, when a halo gets stripped V_{max} changes less dramatically than the mass, and is therefore a better “label” of the halo. For isolated halos, V_{max} and the halo’s virial mass are directly related.

TABLE 1
HALO CATALOGS

z	$V_{max} > 120\text{km/s}$		$V_{max} > 200\text{km/s}$	
	M_{vir}^a	N_{halo}	M_{vir}	N_{halo}
0.0	3.0×10^{11}	4707	1.4×10^{12}	1027
1.0	2.0×10^{11}	7867	9.0×10^{11}	1443
2.0	1.1×10^{11}	10437	5.4×10^{11}	1675
3.0	8.0×10^{10}	9650	3.5×10^{11}	1636

^a Masses are given in $h^{-1} M_\odot$.

For example, a halo with a density distribution described by the Navarro, Frenk & White (hereafter NFW; 1996, 1997) profile $\rho(r) \propto x^{-1}(1+x)^{-2}$ ($x \equiv r/R_s$; R_s is the scale-radius):

$$V_{max}^2 = \frac{GM_{vir}}{R_{vir}} \frac{c}{f(c)} \frac{f(2)}{2}; \quad (12)$$

where M_{vir} and R_{vir} are the virial mass and radius, $f(x) \equiv \ln(1+x) - x/(1+x)$, $c \equiv R_{vir}/R_s$. While for the satellite halos V_{max} may not be related to mass in any obvious way, it is still the most physically and observationally motivated halo quantity.

We constructed halo catalogs using thresholds in the maximum circular velocity (i.e. selecting all halos with V_{max} higher than a specified threshold). The cluster-size halos are not explicitly excluded from the halo catalogs. We assume therefore that the center of each cluster can be associated with a central cluster galaxy. The latter (due to the lack of hydrodynamics and other relevant processes) cannot be identified in our simulations in any other way. We limit the extent of these “galaxies” to the central $150h^{-1}$ kpc of the cluster.

The redshift dependency of the relationship between halo mass and V_{max} is expected to evolve because the concentration factor c (see eq. [12]) is expected to evolve with redshift. We use the prescription of NFW to compute the evolution of $c(M, z)$ and to convert V_{max} to the virial mass, but note that this prescription has been found to deviate significantly from the results of numerical simulations (Bullock et al. 1998; Eke, Navarro & Frenk 1998). The values of the virial mass corresponding to the V_{max} thresholds of 120 and 200 km/s used in our analysis and calculated using eq. (12) and the NFW prescription for $c(M, z)$ are given in Table 1. This Table also gives the number of halos at different epochs identified by the halo finder in the simulation box using these thresholds.

5. RESULTS

5.1. Evolution of the power spectrum

Recent numerical and semi-analytical studies have focused on the bias evolution as determined from the 2-point correlation function. However, as new, accurate measurements of the power spectrum at both low (e.g.,

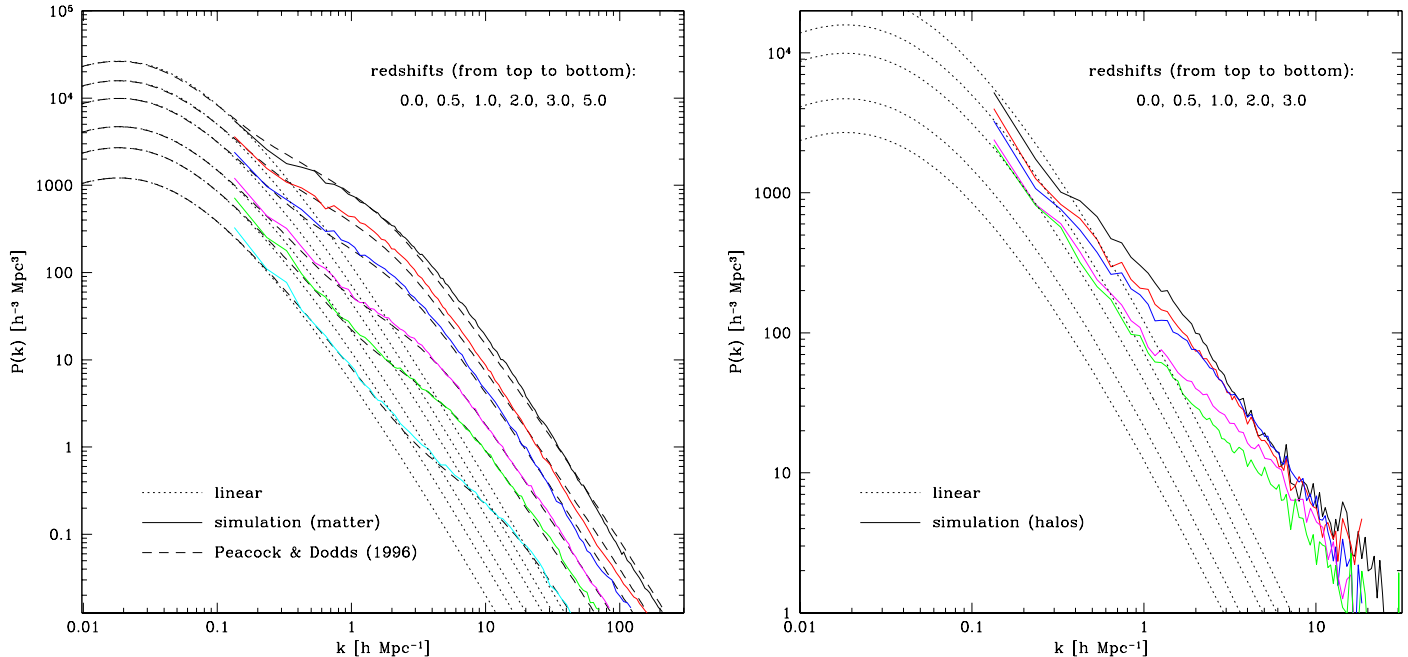


FIG. 1.— Evolution of the (a) matter and (b) halo power spectra. Panel (a): the dark matter power spectra, $P_m(k)$, at different redshifts (*solid lines*) are compared with the linear spectra (*dotted lines*) and predictions of the Peacock & Dodds (1996) fitting formula (*dashed lines*; see text for details). Note that the power spectra in the simulations agree with the analytical predictions at all scales, including highly non-linear scales at which the “stable clustering” approximation appears to work well. Panel (b): evolution of the power spectrum for halos with maximum circular velocities > 120 km/s (*solid lines*) as compared to the linear evolution of the matter power spectrum, $P_m(k)$, is much slower than that of the matter spectrum, $P_m(k)$, shown in panel (a). At high redshifts the amplitude of $P_h(k)$ exceeds that of $P_m(k)$ by a factor of $\sim 5 - 10$, while at lower redshifts the differences are smaller. The ratio of amplitudes, $P_h(k)/P_m(k)$, depends on the scale. These differences imply that the halo bias is time- and scale-dependent.

Baugh & Efstathiou 1993, BE93; Gaztañaga & Baugh 1998, GB98; Tadros & Efstathiou 1996, TE96; Hoyle et al. 1998) and high (Croft et al. 1998; Weinberg et al. 1998) redshifts become available, it is also useful to examine and compare the evolution of the power spectra of matter, $P_m(k)$, and halo, $P_h(k)$, distributions.

Figure 1 shows the evolution of *real-space* $P_m(k)$ and $P_h(k)$ in our simulation. The halo power spectrum is shown for the halo catalog with the maximum circular velocity threshold of $V_{max} > 120$ km/s. To estimate the power spectra over a wide range of wavenumbers, we have used the method of Jenkins et al. (1998a). Both $P_m(k)$ and $P_h(k)$ have been obtained by combining a series of spectra, $\{P_i(k)\}$, in overlapping ranges of k : $[k_{max}^{i-1}, k_{max}^i]$, where k_{max}^i is the maximum wavenumber at which an accurate estimate of the $P_i(k)$ can be obtained. To compute $P_i(k)$, the computational cube (of size L_{box}) is divided into i^3 subcubes and the particle (or halo) distributions in these subcubes are superposed. The FFT of the resulting density field, estimated using the cloud-in-cell density assignment scheme (Hockney & Eastwood 1981), gives an accurate estimate of the power spectrum in modes that are periodic on scale the L_{box}/i . We have used the FFTs on a 256^3 grid, and $i = 2^m$, where $m = 0, \dots, 6$ and $m = 0, \dots, 4$ for the dark matter and halos, respectively. Comparisons with direct 512^3 -grid FFT spectra suggested the use of $k_{max}^i = k_{Ny}^i/6$, where $k_{Ny}^i = 128i(2\pi/L_{box})$ is the Nyquist wavenumber for $P_i(k)$ ($k_{max}^0 = 2\pi/L_{box}$). The individual

power spectra have been corrected for the shot noise by subtracting the noise spectrum estimated using the same method.

Panel (a) of figure 1 shows the evolution of the matter power spectrum from $z = 5$ to the present. For comparison we also show the non-linear evolution predicted by the fitting formula of Peacock & Dodds (1996, hereafter PD96): $\Delta_{NL}^2(k_{NL}, z) = f_{NL}[\Delta_L^2(k_L)]$, where $\Delta^2(k) = dP(k, z)/d\ln k$ and subscripts L and NL denote linear and non-linear quantities, respectively. The analytical expression for f_{NL} depends on five fitting parameters (see §3.3 in PD96) obtained by fitting the power spectra of the scale-free N -body simulations. Although there are some minor difficulties in applying these fitting results to the realistic models with scale-dependent power-law spectral index (PD96; Smith et al. 1998; Jenkins et al. 1998a), the prediction works remarkably well. We have been able to match the non-linear spectra in our simulation at all epochs with only small change in the fitting parameters of PD96. Namely, we have used $n_{eff}(k_L) = d\ln P(k)/d\ln k|_{k_L}$ (as opposed to an alternative $n_{eff}(k_L/2)$) for the estimate of the spectral index at wavenumber k_L and slightly changed the power-index dependence for the fitting parameter V . This parameter controls the amplitude of the high- k asymptote; instead of using $V = 11.55(1 + n_{eff}/3)^{-\eta}$, with a single time-independent value of $\eta = 0.423$ given by PD96, we use η varying from 0.7 at $z = 5$ to 0.45 at $z = 0$. The PD96 for-

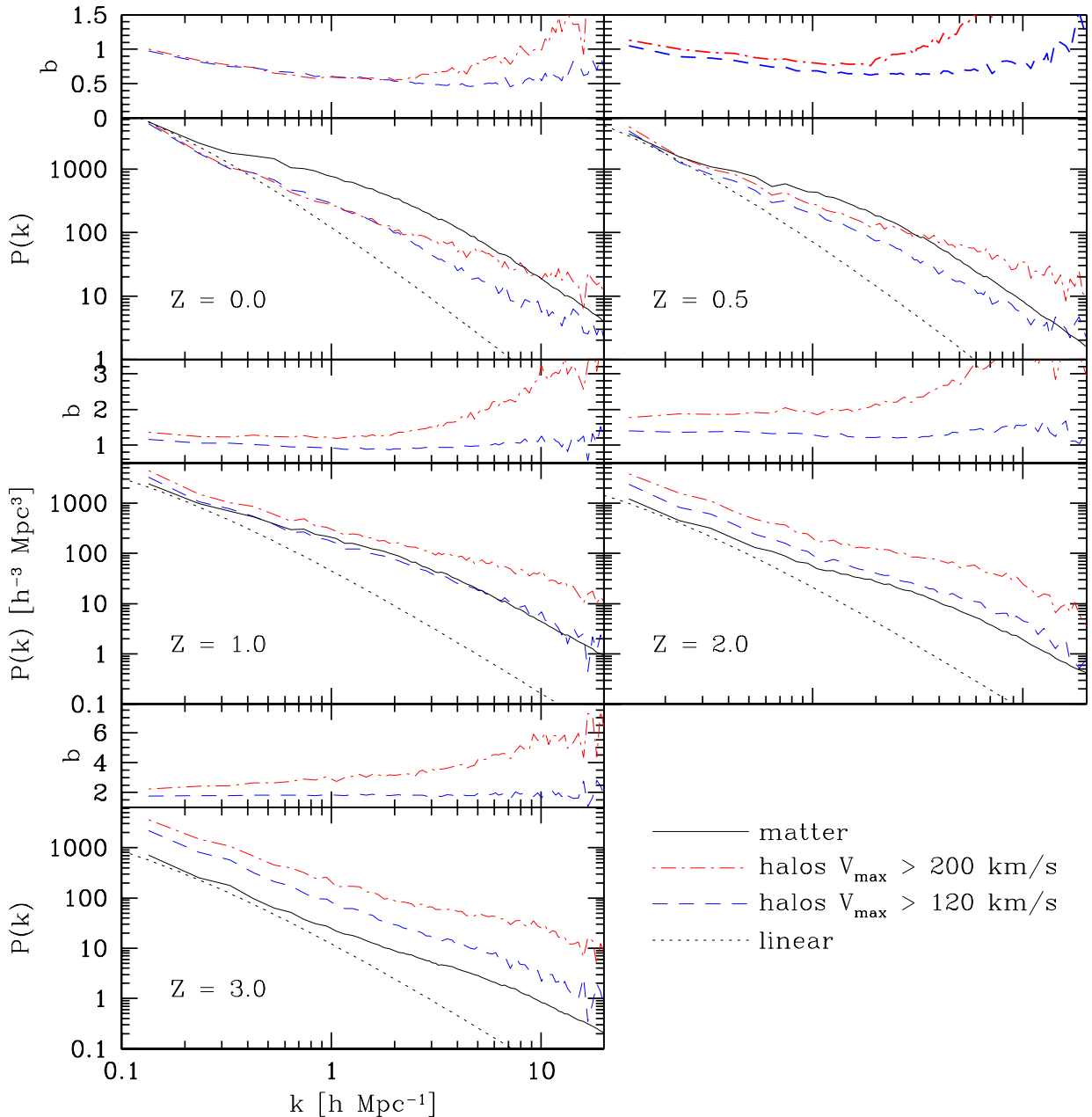


FIG. 2.— Evolution of the halo bias from $z = 3.0$ to the present. The lower portion of each panel shows linear (*dotted lines*) and non-linear (*solid lines*) spectra of the matter distribution compared to the halo power spectra for catalogs with two different lower cutoffs in maximum circular velocity: > 120 km/s and > 200 km/s (shown by *dashed* and *dot-dashed* lines, respectively). The upper portion shows the corresponding bias $b(k) \equiv [P_h(k)/P_m(k)]^{1/2}$.

mula, with their fitting parameters unchanged, fares well at $z < 1$, but underpredicts the amplitude of the asymptote at high z . Figure 1a shows that, with this small modification¹, the PD96 prediction is a success. Nevertheless, if the desired accuracy of the non-linear spectrum estimate is $\lesssim 50\%$, the necessity of such (generally time- and cosmology-dependent) modifications should be kept in mind.

Figure 1b shows that the evolution of $P_h(k)$ is much slower than the evolution of the matter power spectrum. Although the scale of non-linearity (wavenumber of an upward inflection of $P_h(k)$) is seen clearly in the halo spectra and approximately matches the corresponding scale in $P_m(k)$ at the same epoch, the shapes of the halo and matter power spectra are quite different: the $P_h(k)$, for example, can be approximated well by simple power-law,

¹This modification is, of course, arbitrary and the same result could possibly be achieved with other changes; for example, by varying the wavenumber at which n_{eff} is computed.

while the shape of $P_m(k)$ is more complicated. This difference, together with the difference in the evolution rate, means that the bias of the halo distribution is time- and scale-dependent. A similar conclusion has been reached by many researchers from comparisons of halo and matter two-point correlation functions (e.g., recently, Bagla 1998; Colín et al. 1998; Kauffmann et al. 1998ab; Katz, Hernquist & Weinberg 1998; and references therein). Note, however, that as we mentioned in §1, the scale-dependence of the bias is different in real- and k -space (see eq.[4]). Although we will be referring to both $b_P(k)$ and $b_\xi(r)$ (defined in eqs. [1] and [2]) as the bias functions, it should be kept in mind that they have different functional forms.

Figure 2 shows the evolution of the halo bias, $b(k) \equiv [P_h(k)/P_m(k)]^{1/2}$, from $z = 3.0$ to the present epoch for two halo catalogs selected with low and high-mass thresholds: $V_{max} > 120$ km/s and $V_{max} > 200$ km/s. The bias evolves from a value of $\approx 2 - 4$ at $z = 3$ to ≈ 1 at $z = 0$. At high redshifts, the bias depends on the selection threshold indicating that it is mass-dependent; the differences, however, become progressively smaller for lower redshifts. Also, the scale-dependence of the bias of the lower-mass halos, albeit being redshift-dependent and generally $\neq 1$, is significantly weaker than the scale-dependence of the higher-mass halos. At $z = 1$, for instance, the power spectrum of $V_{max} > 120$ km/s halos follows that of the mass almost exactly at all probed wavenumbers. In agreement with analytical prediction of Scherrer & Weinberg (1998), the bias is virtually scale-independent at linear scales $k < k_{nl}$, where k_{nl} is the wavenumber where the $P_m(k)$ becomes non-linear and exceeds the linear prediction ($k_{nl} \approx 0.2 - 0.4$). Note also that during the evolution the bias at these linear scales is driven to the value of ≈ 1 , as expected in the linear regime (Tegmark & Peebles 1998). This is true for both low- and high-mass catalogs, which indicates that the bias evolution at these scales is driven by gravitational growth of clustering that tends to erase any initial (mass-dependent) differences in the halo and mass distributions (Tegmark & Peebles 1998).

The bias evolution at non-linear ($k > k_{nl}$) scales is more complicated. The bias evolves to values less than unity at $z < 1$, and its scale-dependence becomes progressively stronger over a wider range of wavenumbers. We will discuss the possible interpretation of the bias evolution in the non-linear regime in the following section. However, we would like to point out here that the net result of this evolution is the $P_h(k)$ at $z = 0$ which is *significantly anti-biased* with respect to the overall matter distribution but which agrees very well with the power spectrum of observed galaxy distribution. Figure 3 compares the $z = 0$ power spectra of halos and matter in our simulation with the power spectrum of galaxies (BE93; GB98; TE96) in the APM survey. At small scales ($k \gtrsim 2h\text{Mpc}^{-1}$), the $P_h(k)$ depends on the catalog's V_{max} threshold. The galaxy power spectrum, however, lies comfortably in between two likely possibilities of galaxy mass cutoffs. The maximum circular velocities of 120 and 200 km/s correspond at $z = 0$ to the virial masses of $\approx 3 \times 10^{11}h^{-1} M_\odot$ and $\approx 1.5 \times 10^{12}h^{-1} M_\odot$, respectively. At larger scales, the power spectra of halos and galaxies agree within the errors. The “inflection” in the galaxy power spectrum (GB98) is reproduced at the correct wavenumber of $k \approx 0.2h\text{Mpc}^{-1}$.

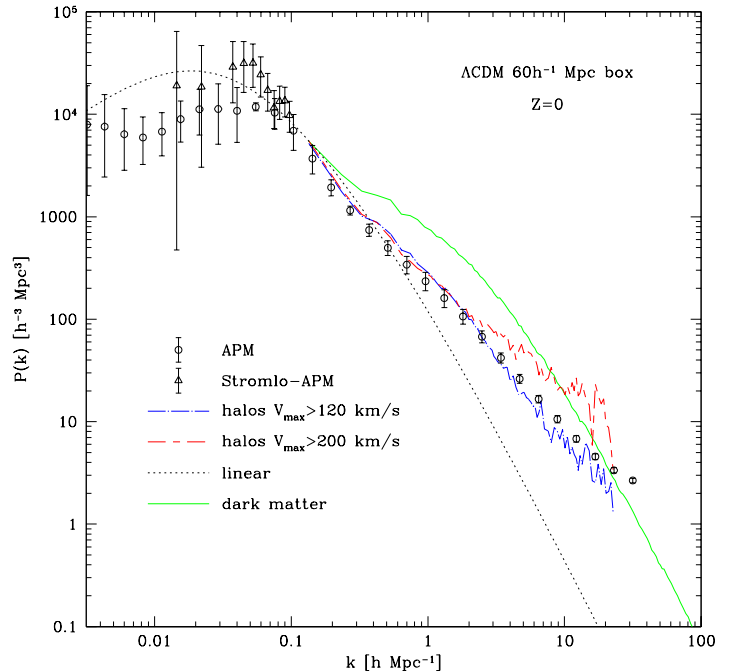


FIG. 3.— Comparison of the $z = 0$ power spectra of the matter (solid line) and halo (dashed and dot-dashed lines) distributions with the galaxy power spectra estimated using the APM (Gaztañaga & Baugh 1998) and Stromlo-APM surveys (Tadros & Efstathiou 1996); the latter is measured in *redshift space* and must be reduced by $\approx 40\%$ to correct out the redshift-space effects (see §5.1 for details). The errorbars of the galaxy power spectra are 2σ . For clarity, the Stromlo-APM power spectrum is shown only at $k < 0.1h\text{Mpc}^{-1}$. Note that the halo power spectrum, $P_h(k)$, matches the galaxy power spectrum significantly better than does the spectrum of the overall matter distribution, $P_m(k)$. Both galaxy and halo distributions are *anti-biased* at $k \sim 0.2 - 10\text{Mpc}^{-1}$; the $P_h(k)$ at these scales has a shape and amplitude different from those of $P_m(k)$. At larger scales, $k \lesssim 0.2\text{Mpc}^{-1}$, the halo distribution is approximately unbiased.

We interpret the “inflection” wavenumber in the observed spectrum as the scale of non-linearity, because both halo and matter power spectra in the simulation become non-linear at higher k . The amplitude of the matter power spectrum at these k , however, is $\sim 3 - 4$ times higher and does not come anywhere close to matching the observed power spectrum. This shows clearly that it is crucial to consider the distribution of halos, not matter, when comparing model predictions to the observations.

It is not clear whether the power spectrum in the ΛCDM model considered here can reproduce the amplitude and shape of the turnover observed in the galaxy power spectrum at $k \sim 0.01 - 0.06h\text{Mpc}^{-1}$. Figure 3 shows that the ΛCDM spectrum does not reproduce the turnover in the spectrum recovered from the APM angular correlation function (BE93, GB98); however, it is in better agreement with the power spectrum derived by TE96 from the Stromlo-APM redshift survey. Also, recently published power spectrum of the Durham/UKST survey (Hoyle et al. 1998) agrees very well with the Stromlo-APM spectrum and with the spectrum of the ΛCDM model. The Stromlo-

APM and Durham/UKST spectra have been computed in *redshift-space*, but the differences from the real-space spectrum *in the Λ CDM model* at these scales are expected to be $\lesssim 40\%$ (TE96; Smith et al. 1998). Even with the 40% lower amplitude, the spectra are in agreement with the model and, within 2σ errors, with the APM power spectrum. The latter indicates either that there are systematic differences between the galaxy surveys or that the cosmological model is incorrect (because it predicts an incorrect redshift-to-real space correction). There is also a possibility that the amplitude and errors of the APM power spectrum are somewhat underestimated at these large scales (Peacock 1997). Unfortunately, at present, statistical and systematic observational errors are too large at these scales to be able to make a decisive conclusion. In any case, considering the whole range of observationally probed wavenumbers, the agreement between the data and the model is much better when we compare observations to $P_h(k)$, as opposed to $P_m(k)$.

5.2. Overdensity of matter vs. overdensity of halos

5.2.1. Linear and mildly non-linear overdensities

The evolution of bias, as determined from the power spectra in the previous section, agrees qualitatively with the bias evolution derived from the correlation function analyses (e.g., recently, Bagla 1998; Colín et al. 1998; Kauffman et al. 1998ab; Katz, Hernquist & Weinberg 1998; and references therein). The bias functions $b_P(k) \equiv \sqrt{P_h(k)/P_m(k)}$ and $b_\xi(r) \equiv \sqrt{\xi_h(r)/\xi_m(r)}$ (see §5.1), defined using the power spectrum and the correlation function, illustrate the scale dependence of the bias. However, it is difficult to interpret b_P and b_ξ in terms of the most generic definition of bias²: $\delta_h = b_\delta \delta_m$, where we denote the bias in this definition by b_δ to distinguish it explicitly from b_P and b_ξ . The b_δ shows how bias depends on the matter density at a fixed scale, the information which cannot be extracted easily from b_ξ and b_P . Therefore, to get a full picture of the bias evolution, we examine the evolution of b_δ in our simulation.

To estimate δ_h and δ_m , we use the top-hat filter (see §2) of *comoving* radius $R = 5h^{-1}$ Mpc. The size of the radius is a compromise between halo statistics and the range of probed overdensities. Note that our simulation box contains only 216 independent spheres of this size. This is the maximum number of spheres that can be used to study the scatter of the bias. However, we are primarily interested in the average behavior of b_δ ; therefore, in order to probe the wide range of overdensities, we use a large number (50,000) of spheres, placed randomly throughout the simulation box. To calculate δ_h , we have used halos with maximum circular velocities of $V_{max} > 120$ km/s. Due to limited mass resolution, the halo catalogs are somewhat incomplete for $V_{max} \lesssim 100$ km/s (see Gottlöber, Klypin & Kravtsov 1998). The catalog with the threshold of 120 km/s is complete and contains a large enough number of halos (see Table 1) to provide sufficient statistics.

Figure 4 shows overdensity of dark matter halos, δ_h , as a function of matter overdensity δ_m at four epochs: $z = 0, 1, 2, 3$. The solid curves show the *average* relation,

calculated by averaging δ_h of the individual spheres in bins of δ_m . The actual binned distribution of the δ_m and δ_h values is shown by grey-scale shades on a grid, where the intensity of grey corresponds to the natural logarithm of the density of points in the grid cell. The figure shows that at all epochs, the halo overdensity is tightly correlated with the overdensity of matter. However, the slope of the correlation, the bias, depends on δ_m (i.e., the bias is non-linear) and changes non-trivially with time.

The dashed and dot-dashed lines in each panel of Figure 4 show predictions of the analytical model of bias described in §2 (namely, eqs. [8] and [9]). To account for the range of halo masses used in our halo catalog, we calculate the mass function weighted bias (eq. [11]) using $M_{max} = 10^{13}h^{-1} M_\odot$ as an upper limit of integration, and redshift-dependent $M_{min}(z)$ corresponding to our selection threshold of maximum circular velocity of 120 km/s (see §3 and Table 1).

The two model curves correspond to different assumptions about formation redshift of halos, z_f : $z_f = z$ (i.e., halos forming at the epoch of observation) for the dot-dashed curve and $z_f = z + 1$ for the dashed curve. In the standard Press-Schechter model, hierarchical build-up of halos is a continuous process and, therefore, if mass is considered as a defining property of a halo, $z_f = z$. However, this interpretation fails if halos can retain their identity over a finite period of time (e.g., see discussion in Moscardini et al. 1998). For example, if a halo is accreted by a more massive system and orbits in the system's potential instead of merging instantly, it can be identified at $z < z_f$. The galaxy-conserving model of bias evolution (e.g., Moscardini et al. 1998 and references therein) represents an extreme in which halos are never destroyed after being formed and in which the halo clustering is driven solely by the gravitational pull from the surrounding growing structures.

In reality, we expect the merging to take place and the halos to have individual merging histories and thus individual *survival times*³ (Lacey & Cole 1993; Kitayama & Suto 1996). A rigorous treatment of bias should therefore take into account only the halos that survive until the epoch of observation z . In practice, this is a difficult task: although the halo formation epoch is well defined, definition of the halo destruction is not trivial. Lacey & Cole (1993) define halo lifetime as the period between formation time of a halo and the time by which this halo is incorporated into a more massive system. This definition differs significantly from how we define the destruction when analyzing the simulations: the halo is destroyed either when it merges with another halo and loses its identity or when the tidal stripping brings the mass bound to the halo below some mass threshold (defined as a selection criterion or by the mass resolution of the simulation). Therefore, for illustration purposes, we will treat z_f as a free parameter, leaving a more rigorous treatment for future work.

Figure 4 shows that different assumptions about z_f lead to significant difference in the behavior of bias predicted by eq. (9). Although at $\delta_m \lesssim 0.5$ the two bias predictions are similar, at higher overdensities they di-

²All definitions are, of course, equivalent if the bias is linear. This, however, is not true for the non-linear bias, which appears to be a generic feature of the CDM models.

³The survival time is the time between halo formation and destruction.

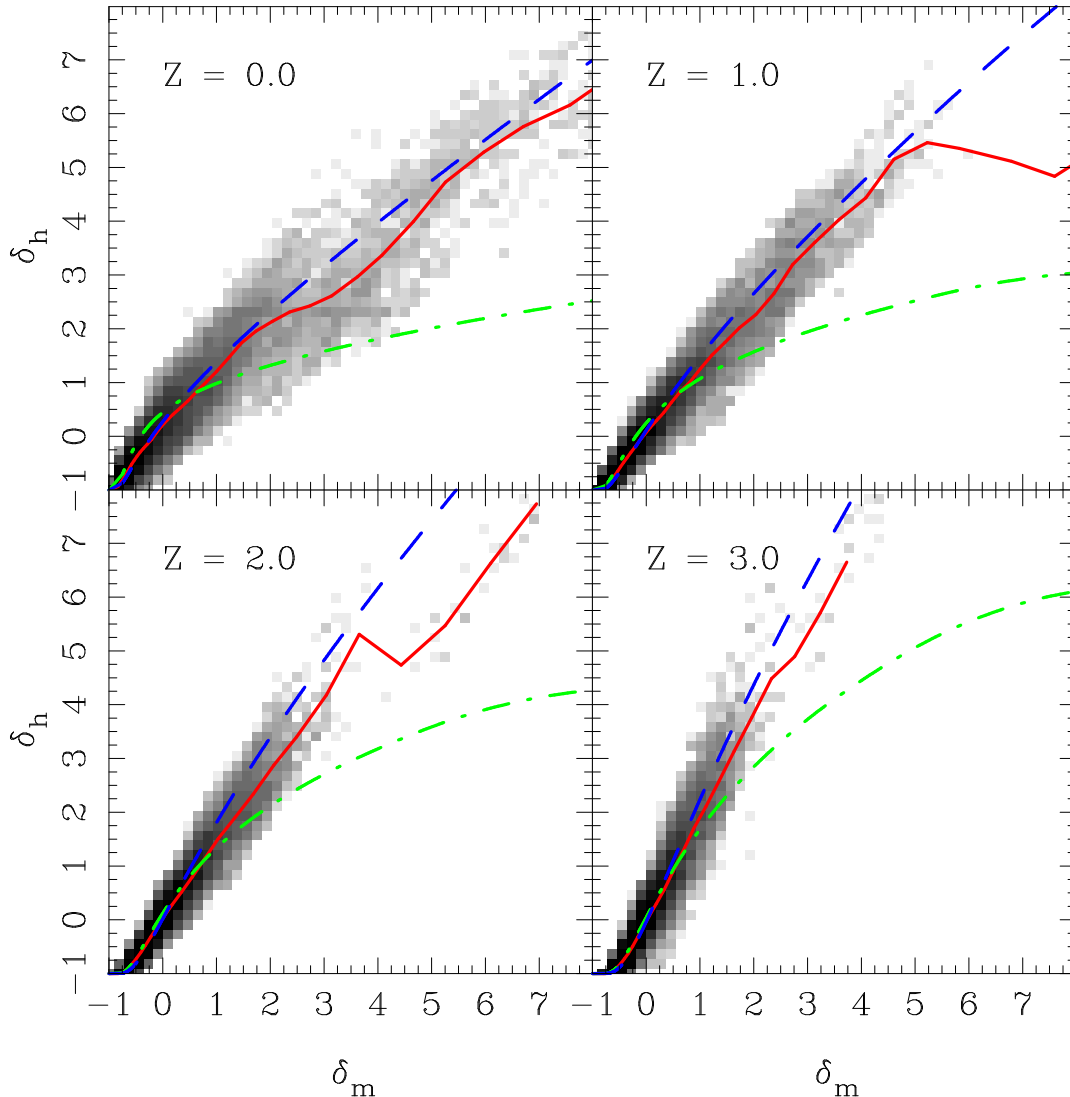


FIG. 4.— The overdensity of halos δ_h vs. the overdensity of matter δ_m at different epochs (indicated on each panel). Both overdensities have been estimated in spheres of radius $R_{\text{TH}} = 5h^{-1}$ Mpc randomly placed in the simulation box. The solid curves show the *average* relation, calculated by averaging δ_h of the individual spheres in bins of δ_m . The actual binned distribution of the δ_m and δ_h values is shown by the shades of grey on a 2D grid, where the intensity of grey corresponds to the natural logarithm of the number of spheres in this grid cell. The *long-dashed* and *dot-dashed* curves show predictions of the analytical model described in §2. The dot-dashed curve is a prediction of the model assuming that formation redshift coincides with observation redshift ($z_f = z$), while the long-dashed curve corresponds to assumption $z_f = z + 1$ (see §5.2 for details). The figure shows that at all epochs halo overdensity is tightly correlated with overdensity of matter. However, the slope of the correlation, the bias, depends on δ_m (i.e., the bias is non-linear) and changes non-trivially with time. Note that at $z > 1$ the halo distribution is biased in overdense regions ($\delta_m \gtrsim 0$) but is anti-biased in underdense regions ($\delta_m \lesssim -0.5$). At low-redshift there is an anti-bias at high-overdensities and almost no bias at low overdensities (see §6 for discussion).

verge, the $z_f = z + 1$ assumption providing a much better match to the simulation results. Note that $z_f = z$ underestimates the bias in the simulation at $\delta_m \gtrsim 1$. This was noted recently by Jing (1998) who studied mass- and scale-dependence of bias in the linear regime. For the simulation of the Λ CDM model used in this paper, Jing finds that halos of mass $10^{11}h^{-1} M_\odot$ exhibit bias of $b^2(M = 10^{11}h^{-1} M_\odot) \approx 0.5 - 0.6$, while *linear* MW bias is (eq. [10] assuming $z = z_f$): $b_L^2 \approx 0.28$. For the same halo mass and $z_f = z + 1 = 1$, eq. (10) gives $b_L^2 \approx 0.67$,

and therefore the finite survival time of halos may naturally explain the bias discrepancy. It is worth noting that for cluster halos, the b_L with $z_f = z$ provides a considerably better approximation which likely reflects late cluster formation ($z \approx z_f$) and/or smaller survival times for cluster-size halos, as is indeed predicted by the extended Press-Schechter theory (Lacey & Cole 1993).

5.2.2. Non-linear overdensities

Figure 5 shows the present-day δ_h - δ_m relation at higher overdensities. Although we use a large number of spheres

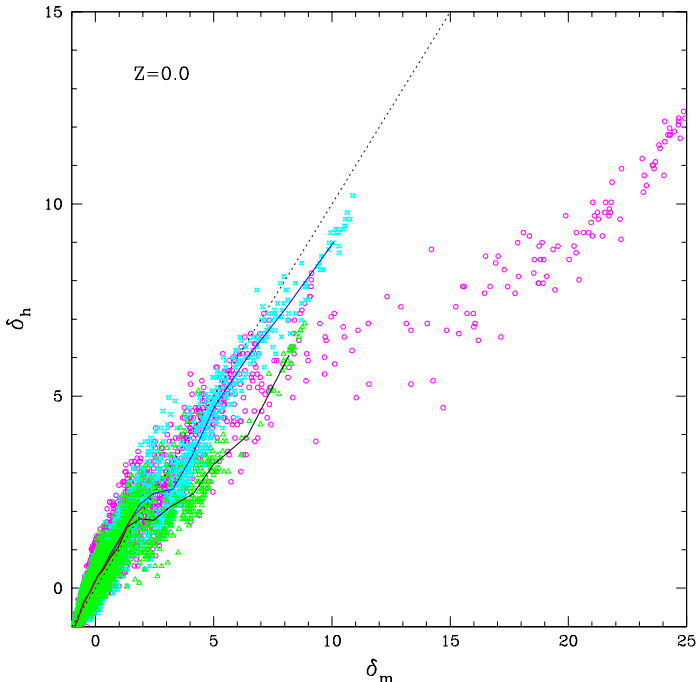


FIG. 5.— The overdensity of halos δ_h vs. the overdensity of matter δ_m at $z = 0$ in spheres of radius $R_{\text{TH}} = 5h^{-1}$ Mpc randomly placed in the simulation box. The different symbols correspond to the spheres in three independent (non-overlapping) sub-cubes of the simulation volume (sub-cube size of $30h^{-1}$ Mpc) that contain most of the massive clusters in the simulation. The lines represent the average relations for the sub-cubes marked with triangles and crosses. Notice the differences in δ_h vs. δ_m correlation at high δ_m . We attribute these differences to the differences in formation histories of structure in these sub-cubes (see §6 for details). The anti-bias at very high overdensities ($\delta_m \gtrsim 10$) arises in a region surrounding the richest Coma-size cluster in the simulation.

and oversample the density field, the spheres in independent regions of space are independent and may thus give an idea about the true scatter in the halo bias. In order to study this scatter, we have divided the computational box into eight equal-size ($30h^{-1}$ Mpc) non-overlapping sub-cubes. Different symbols (of different colors) in Figure 5 correspond to spheres in the three sub-cubes that contain most of the massive clusters in the simulation at $z = 0$. The other five sub-cubes contain lower density regions and are not shown for clarity.

Figure 5 shows that the differences between δ_h - δ_m relations in different sub-cubes are significantly larger than the scatter of each individual relation. Note, however, that even within a single sub-cube there are indications of real scatter: the sub-cube represented by the triangle markers shows a dichotomy of δ_h at fixed $\delta_m \approx 2 - 4$. Analysis of the sub-cubes has shown that differences in the δ_h - δ_m correlation among the sub-cubes are real and are caused by the differences in the non-linear structures they contain.

It appears that the scatter and the differences can be explained by the following two effects. The centers of the spheres with $\delta_m \gtrsim 5$ fall preferentially in close vicinity to the massive group- and cluster-size halos. These cluster halos span a wide range of masses and, most importantly,

formation times. The differences in formation times result in different fates of dark matter halos orbiting inside these clusters. If, for example, a cluster forms and accretes the bulk of its mass and halos early, the halos have time to suffer substantial losses of mass due to tidal stripping and losses of orbital energy from dynamical friction. Dynamical friction may lead to a merging between satellite and central cluster object, thus resulting in a “loss” of the satellite. Tidal stripping may lead to a substantial mass loss and may ultimately (although at a much slower rate) decrease the halo’s maximum circular velocity (see KGKK) bringing the halo below our threshold V_{max} . These effects are enhanced because the virial radius is smaller at earlier epochs and so are the typical pericenters of satellite orbits. If, on the other hand, the cluster forms late and accretes most of its mass fast and at relatively low redshifts, the halos are accreted onto a massive cluster and thus have higher orbital energies and orbits with larger pericenters. Moreover, many halos simply do not have enough time to suffer substantial tidal or orbital energy losses.

The differences in formation histories may therefore lead to significant differences in the halo content among clusters. This is illustrated in Figure 6 which shows “bias profiles”: the ratios of the *integral* overdensities of halos and matter in spheres of increasing radii centered on a cluster. The profiles for 5 of the clusters from the three sub-cubes of Figure 5 are shown at three different epochs $z = 0.0, 0.5, 1.0$. Note the large differences between profiles at $z = 1$. While the cluster marked CL1 exhibits strong *anti-bias* (i.e., low δ_h/δ_m), the halos in cluster CL2 are strongly biased. Similar differences are seen in the rest of clusters. Interesting differences can also be observed in the subsequent evolution of $b(r)$. Cluster CL1 shows very mild evolution in $b(r)$ at small ($r \lesssim 1h^{-1}$ Mpc) scales, whereas other clusters show very strong evolution between $z = 1.0$ and $z = 0.5$, and much weaker evolution from $z = 0.5$ until present.

The changes in the rate of evolution may seem counterintuitive; indeed, the time period corresponding to the $z = 1.0 - 0.5$ interval is approximately twice as short (≈ 2.5 Gyrs) as the period between $z = 0.5$ and $z = 0$ (≈ 5 Gyrs). We could thus expect more significant changes at $z < 0.5$ due to more prolonged effects of tidal stripping and dynamical friction. However, as we have noted above, as the mass of a cluster grows with time, the halos are accreted on higher-pericenter, higher-energy orbits and thus are not as likely to approach the dense central region or spend a substantial amount of time there.

To illustrate that this indeed is the case, we have analyzed the dynamical evolution of halos identified within the virial radius of clusters at different moments in time. Figure 7 shows the evolution of 5 halos randomly selected within the virial radius of cluster CL1 at $z = 3$ (there are a total of 10 halos within the virial radius). At all epochs, CL1 is the most massive cluster in the simulation box; at $z = 3$ its mass was $1.5 \times 10^{13}h^{-1} M_{\odot}$. The panels in each of the horizontal rows in Figure 7, show the evolution of particles that bound to the halos at $z = 3$. The orbits of 4 halos are contained within the cluster virial radius, $\approx 150h^{-1}$ kpc, at $z = 3$ (shown as a circle in each panel), where all of these halos merge with the central $\sim 100h^{-1}$ kpc size object by $z = 1$ (i.e., after ≈ 3.5 Gyrs). The halo on the most eccentric orbit (bottom row) survives

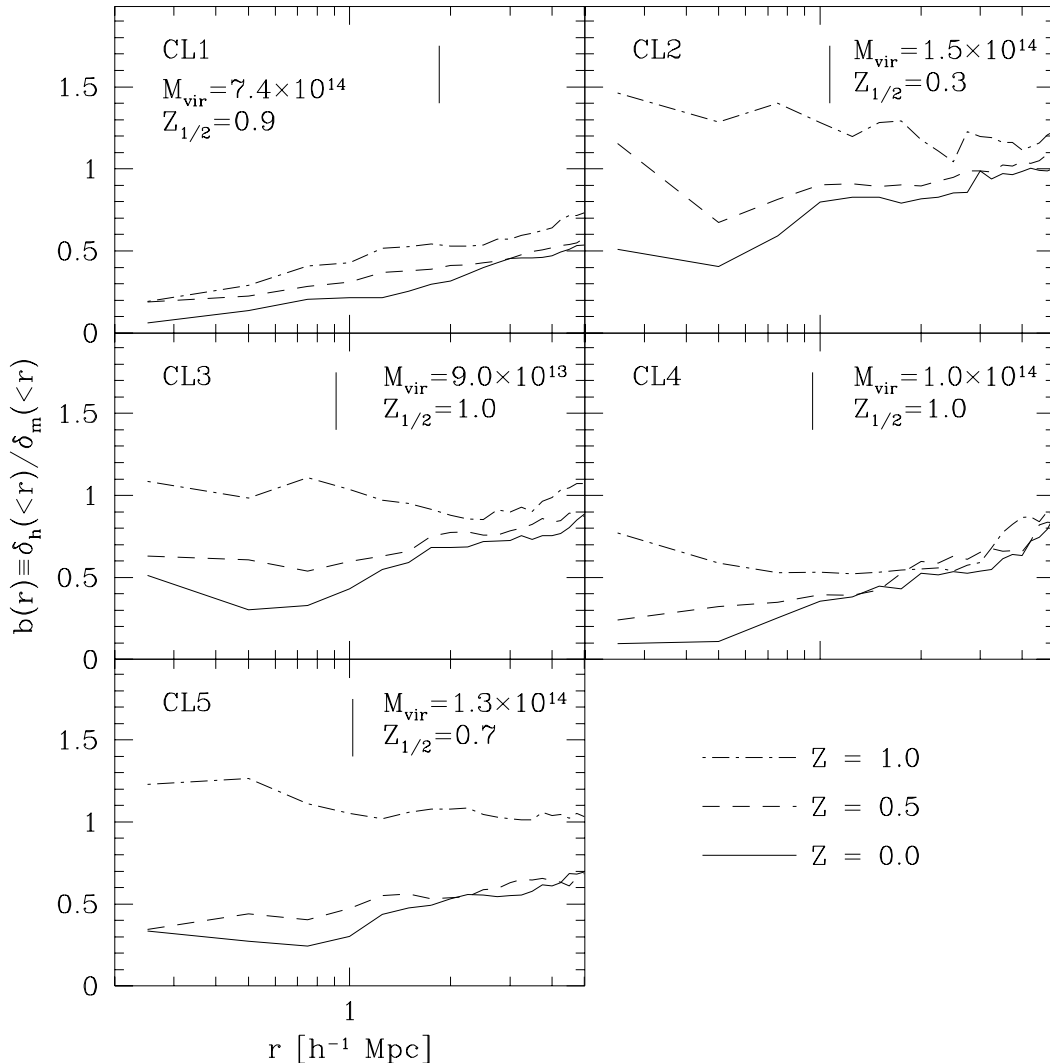


FIG. 6.— Bias profiles (ratio of halo to matter overdensities inside a sphere of radius r centered on the cluster center) of five of the rich ($M_{\text{vir}} \gtrsim 10^{14} h^{-1} M_{\odot}$) clusters from the three sub-cubes shown in Fig. 5 at three different epochs $z = 0.0, 0.5, 1.0$. The vertical lines indicate the virial radii of clusters at $z = 0$; M_{vir} and $Z_{1/2}$ indicate the $z = 0$ virial mass and redshift at which cluster had half of this mass, respectively. Note the large differences between profiles at $z = 1$. While cluster marked CL1, the most massive cluster in the simulation, exhibits strong *anti-bias* (i.e., low δ_h/δ_m), the halos in cluster CL2 are strongly biased. Similar differences are seen in the rest of clusters. Interesting differences can also be observed in the subsequent evolution of $b(r)$. Cluster CL1 shows very mild evolution in $b(r)$ at small ($r \lesssim 1 h^{-1}$ Mpc) scales, whereas other clusters show very strong evolution between $z = 1$ and $z = 0.5$, and much weaker evolution from $z = 0.5$ until present.

until $z \approx 0.5$ and gets tidally destroyed after that.

For comparison, Figure 8 shows the evolution of 10 halos randomly selected within the virial radius of the same cluster CL1 at $z = 0.5$. As before, most of the halos stay within the $z = 0.5$ virial radius ($\approx 1.2 h^{-1}$ Mpc). However, unlike the $z = 3$ halos, most of them (8 out of 10) survive until $z = 0$ (i.e., during the period of ≈ 5 Gyrs). Although some halos suffer substantial mass loss in their outer regions, the dense halo cores can be identified at $z = 0$. Note that two halos on low-pericenter orbits do merge with the central object.

Finally, we have also visually examined the fate of the halos identified in cluster CL5 of Fig. 6 at $z = 1$ and $z = 0.5$. More than half of the $z = 1$ halos merge with the

central object by $z = 0.5$, while most of the $z = 0.5$ halos survive until $z = 0$. The difference is caused by both the lower typical orbit pericenters at higher redshifts and the higher efficiency of the dynamical friction due to a smaller mass of cluster. It explains the evolution of the bias profile shown in Fig. 6.

To illustrate the relative efficiency of dynamical friction at different epochs of cluster evolution, we present the evolution of the dynamical friction time-scale in a cluster. At a given epoch, the dynamical friction time, t_{fric} , can be estimated using Chandrasekhar’s formula (Binney & Tremaine 1987), assuming the cluster mass and density distribution and the mass of the satellite. In the right column of Figure 9, we present estimates of t_{fric} for ha-

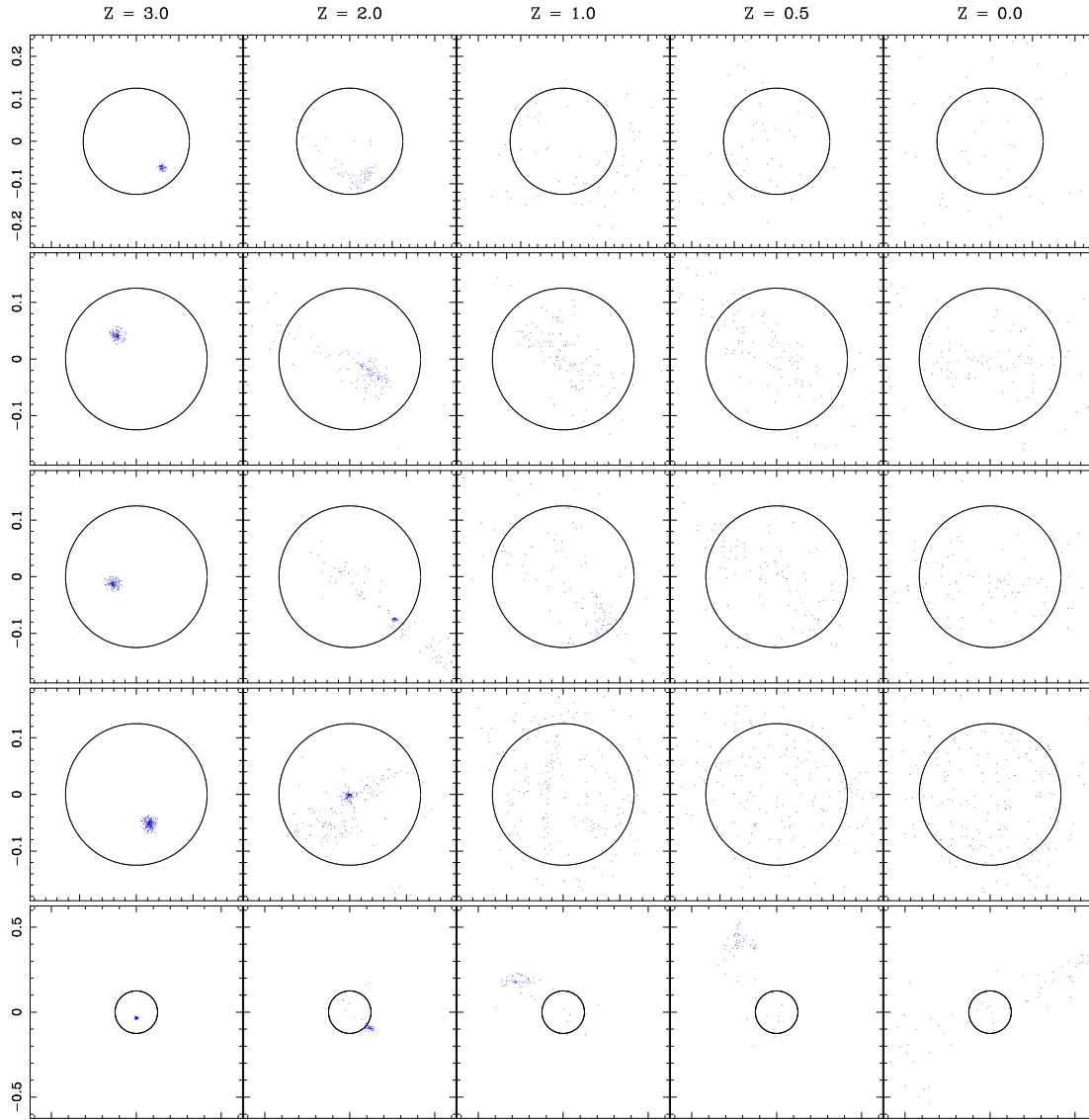


FIG. 7.— The leftmost column of panels shows particles bound to the five halos identified within the virial radius of the cluster CL1 shown in Fig. 6 at $z = 3$ ($R_{\text{vir}} \approx 120h^{-1}$ kpc (proper) and $M_{\text{vir}} \approx 1.5 \times 10^{13}h^{-1} M_{\odot}$ at $z = 3$). The rest of the columns show positions of the same particles at later moments. Four out of five halos merge with the central cluster halo by $z \approx 1$. In all panels particles are plotted in proper coordinates; the circles in all panels have the same radius equal to the virial radius of the cluster at $z = 3$.

los with maximum circular velocity $V_{\text{max}} = 120$ km/s for clusters of different final masses. The mass accretion histories of clusters of similar present-day mass exhibit a spread around an average, typical for this mass, evolution track. To account for this spread, we have used both the average mass evolution tracks and two individual evolution tracks representative of the early- and late-forming tails of the population (these tracks represent $\approx 2\sigma$ deviations from the average mass evolution track). The cluster mass evolution tracks used here (Avila-Reese & Firmani 1997) have been generated using the Monte-Carlo method of Lacey & Cole (1993). For each epoch, we compute t_{fric} using eqs. (8-10) of KGKK assuming the NFW density distribution (with an appropriate $c(M, z)$, see §4) for both the cluster

and satellite at a distance $R_{\text{vir}}/2$ from the cluster center (where R_{vir} is the virial radius of the cluster at this epoch), and accounting explicitly for the mass loss due to the tidal stripping.

The right column of panels in Figure 9 represents the dynamical friction time in a different, easier to interpret, way. It shows the “merging redshift,” defined as the redshift corresponding to the time $t + t_{\text{fric}}$, where t is the current epoch (redshift z). In the sense of the dynamical friction time, z_{merge} can be interpreted as a redshift at which most of the halos present in cluster at redshift z , will merge into a central object. This interpretation assumes that the mass of the cluster would not change, which is not correct. The actual value should therefore be

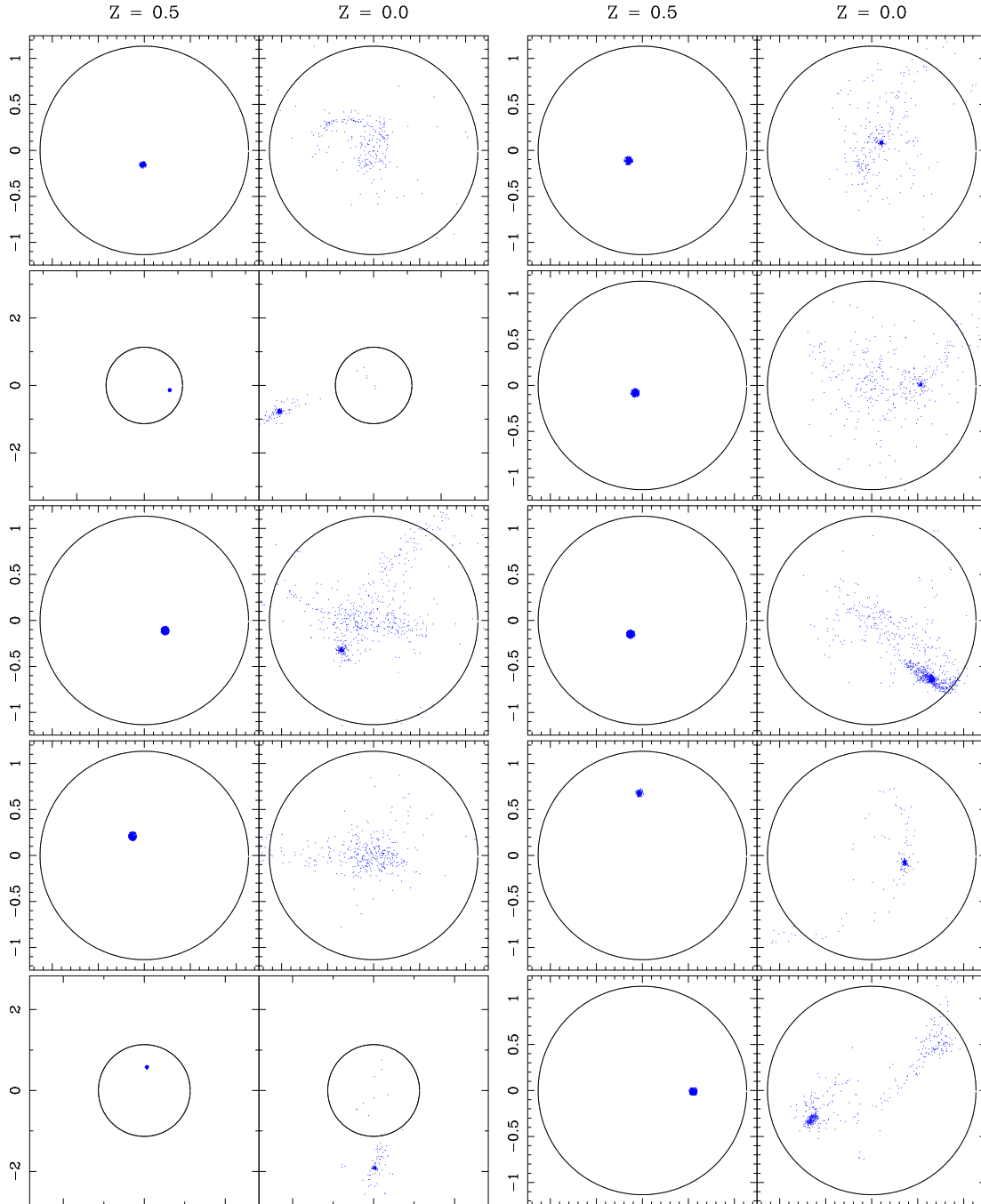


FIG. 8.— The same as in Fig. 7 but for ten halos randomly selected from the halos identified within the virial radius of the cluster at $z = 0.5$ ($R_{\text{vir}} \approx 1.1 h^{-1}$ Mpc (proper) and $M_{\text{vir}} \approx 5.8 \times 10^{14} h^{-1} M_{\odot}$). The first and third columns from the left show the positions of the particles bound to the halos at $z = 0.5$, while the second and the fourth panels show the positions of the same particles at $z = 0$. Note that despite substantial mass losses, eight out of ten of these halos can be identified at $z = 0$ as distinct dense clumps of particles. The circles in all panels have the same radius equal to the virial radius of the cluster at $z = 0.5$.

considered as an upper limit on the actual z_{merge} . Negative values $z_{\text{merger}} < 0$ mean that the dynamical friction time is larger than the time span between redshift z and the present.

Figure 9 shows that regardless of the final cluster mass, dynamical friction is efficient at $z \gtrsim 3$. For small final mass clusters, dynamical friction is efficient throughout the entire cluster evolution, while for medium- and high-mass

clusters, dynamical friction effectively switches off as the cluster exceeds a certain mass threshold. Cluster CL1 in Figure 6, evolves very close to the average mass evolution track of the $6 \times 10^{14} h^{-1} M_{\odot}$ final mass clusters. From the estimate of z_{merge} we can therefore expect that all of its satellite halos will merge into the central object by $z \sim 0.5-1$. Note also that for all cluster masses, only halos accreted before $z = 0.5$ can be substantially influenced by

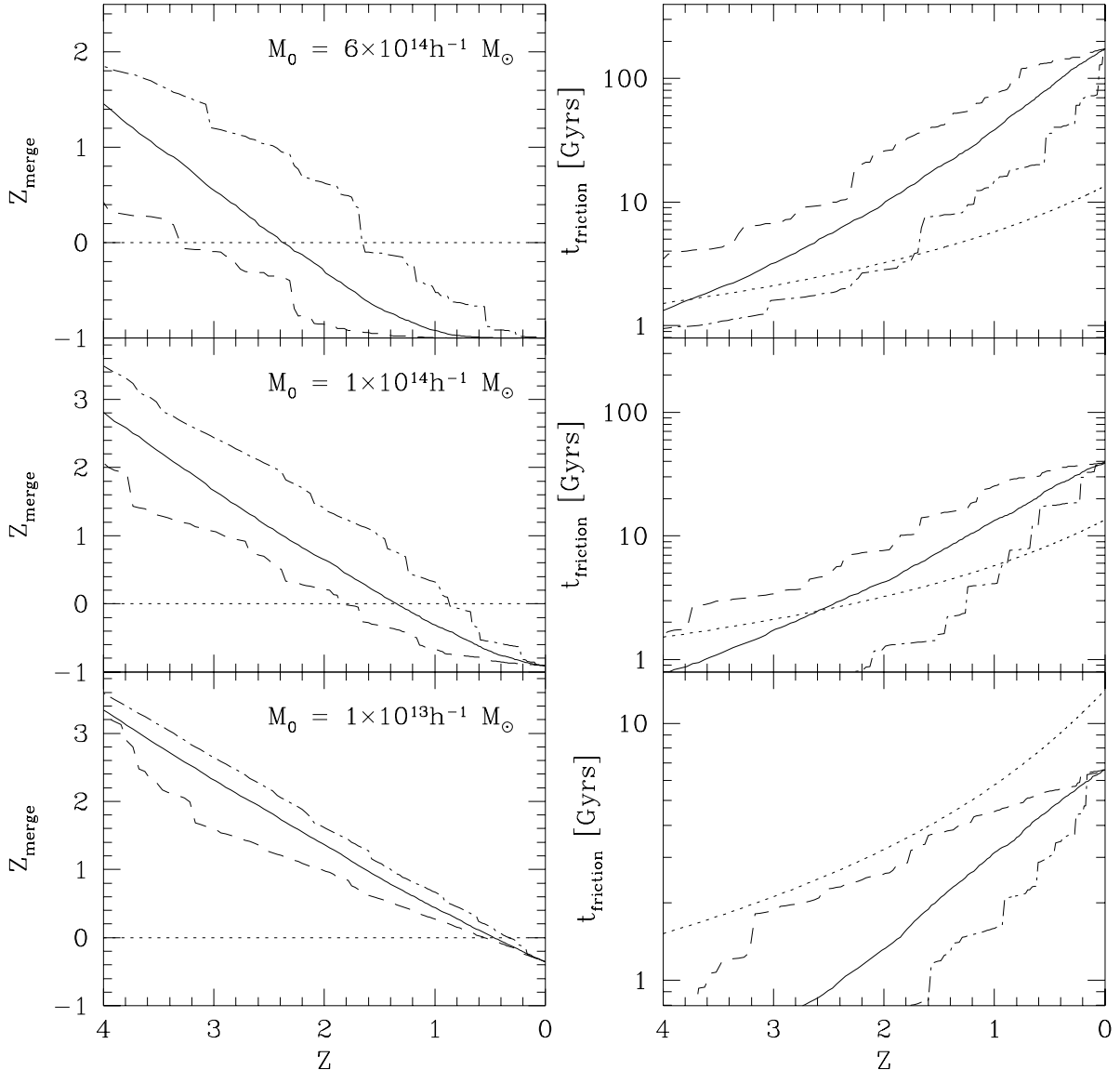


FIG. 9.— Estimates of the dynamical friction time-scale as a function of time for clusters of different final ($z = 0$) mass M_0 . The right column presents estimates of t_{fric} for satellite halos of maximum circular velocity $V_{max} = 120$ km/s. The three curves correspond to the average evolution (solid curves), early formation (dashed curves) and late formation (dot-dashed curves) computed using Monte-Carlo realizations of mass accretion histories (see §5.3 for details). The dotted curve shows the age of the Universe in the Λ CDM model studied here as a function of redshift. The left column shows the corresponding evolution of “merging redshift” defined as a redshift corresponding to $t(z) + t_{fric}(z)$, where $t(z)$ is age of the Universe at redshift z and t_{fric} is the corresponding dynamical friction time-scales (both quantities are shown in the right panel). The curve marking has the same meaning as in the right panel. Negative values $z_{merger} < 0$ mean that the dynamical friction time is larger than the time span between redshift z and the present.

dynamical friction. However, even at $z < 0.5$, dynamical friction may remain efficient in less massive clusters and groups, which, if accreted by a cluster, will be depleted of halos and will tend to lower the bias value further in this cluster. Both of these results are in qualitative agreement with simulation (see Figs. 7,8).

6. DISCUSSION

Results and arguments presented in the previous section suggest that we can identify major processes that drive the evolution of the halo bias. In the linear ($\delta_m \lesssim 1$; the overdensities quoted here and below are for a density

field smoothed with the top-hat filter of radius $R_{TH} = 5h^{-1}$ Mpc) and mildly non-linear regimes ($\delta_m \lesssim 3$) the analytical model of bias developed by Mo & White (1996; see §2) is in good agreement with the results of our simulation, *if* the formation epoch of halos z_f is distinguished from the epoch of observation z (or, in other words, if halos are assumed to retain their identity during a finite interval of time after their formation). This model reproduces the non-linearity and time evolution of the bias observed in the simulation well (see Fig. 4). The evolution of the bias in linear and quasi-linear regimes is, therefore, driven primarily by the halo collapse and merging rates specific

for a given cosmological model.

Interplay between halo formation and the merging rate in high-density regions (affecting $n(M, z, z_f | R_0, \delta_0)$ in eq.[8]) and halo formation and the merging rate in the field (affecting $n(M, z, z_f)$) leads to the decrease of the bias with time *for halos in a given mass range*. This is simply because halos of a given mass collapse earlier in high-density regions than they do in the field; the high-redshift objects therefore represent rare events in the density field and are initially strongly clustered due to modulation by large-scale modes. The number of halos in high-density regions is then decreased due to merging, while number density of halos in the field may still increase (or level off depending on mass range considered) at lower redshifts. The ratio is thus a decreasing function of time. In the regions of negative overdensity ($\delta_m \lesssim -0.5$), the evolution is reverse: formation of halos of a given mass in these regions is delayed and at early epochs their number density is below the average (see Fig. 4). The halos in underdense regions are thus anti-biased at early epochs. Figure 4 shows that bias at $\delta_m \lesssim -0.5$ increases during evolution as the collapse threshold is reaching lower and lower overdensities and more and more halos are being formed in these underdense regions (Fig. 5 shows that $b \approx 1$ for $-1 \lesssim \delta_m \lesssim 2$ at $z = 0$). The prediction of the analytical model at these overdensities matches our numerical results nicely.

In high-density regions ($\delta_m \gtrsim 3$), the evolution and amplitude of bias appears to be significantly affected by dynamical friction⁴. Indeed, the process results in halo mergers with the central cluster halo and reduces thereby the ratio of halo to matter overdensities. The efficiency of dynamical friction depends sensitively on the mass of satellite halos, properties of halo orbits, and mass of the cluster. The latter evolves rapidly with time and switches dynamical friction off at some epoch ($z \sim 0.5 - 1.0$ for the Λ CDM model studied here). The mass accretion history is a stochastic process and some scatter in the mass evolution is expected for clusters that have the same mass at $z = 0$ (Lacey & Cole 1993): some clusters accrete most of the mass early on, while others accrete most of their mass at lower redshifts. Therefore, for a given observation epoch z , different clusters may be affected by the dynamical friction to a different degree. For example, a cluster which have accreted most of its mass (and halos) just prior to z , will be less affected than a cluster of the same mass that accreted most of its halos earlier because dynamical friction had more time to operate in this cluster. The situation is even more complicated, because clusters, even those in which dynamical friction becomes inefficient due to mass increase, may accrete smaller clusters and groups which, in turn, have different evolution histories and therefore different ratios of halo to matter overdensities.

Dynamical friction is not the only process that affects halo counts in clusters and groups. Tidal fields of clusters strip the outer parts of satellite halos which may result in substantial mass loss for a medium- and high-mass clusters (up to a factor of 5 – 20 depending on parameters of

the halo orbit and the period of time the halo spends in cluster; see, e.g., KGKK). The maximum circular velocity, V_{max} , of the halo changes only mildly, even in the case of severe mass loss (which, as a reminder, is the reason we use it for the halo selection). Nevertheless, for some halos V_{max} may decrease below the selection threshold, in which case these halos will “drop out” of the catalogs. This process likely contributes to the mild evolution of bias seen in Fig. 6 at $z \leq 0.5$. The efficiency of tidal stripping is lower for lower-mass systems; therefore, we expect it to be important only in relatively massive ($M_{vir} \gtrsim 10^{14} h^{-1} M_\odot$) clusters. While this effect may seem to depend on the particular halo selection procedure used in our analysis, similar effects may arise for other selection procedures⁵. It is clear, for example, that this effect would be even more severe had we chosen to select halos using their *bound* mass. Observationally, galaxy catalogs are usually selected using a fixed luminosity limit in a given wavelength band. If the luminosity of galaxies in this band evolves differently in clusters than in the field (which is strongly suggested by a variety of observations), the uniform selection criterion is bound to select somewhat different galaxy populations in high- and low-density regions.

Different evolution histories of different systems may result in different locally evaluated bias. If, for example, matter and halo density fields are smoothed at some sufficiently large (larger than typical cluster size) scale, regions of a similar matter overdensity may correspond to different halo overdensities, because the latter depends on the evolution history of systems encompassed within the smoothing scale. We can expect, therefore, that bias evaluated at a finite smoothing scale will exhibit some scatter in different regions of space. Note that this scatter arises not from the “stochasticity” of the halo formation, but from the fact that the same matter overdensity may correspond to regions of very different evolution histories and, thus, of different halo content. On the other hand, the differences in the evolution histories result from the modulation by large-scale modes in the density distribution. The bias is thus also modulated by the large-scale modes and is therefore *non-local*. Note that this “stochasticity” should decrease, as one smooths density fields on progressively larger scales because effects of the modulation by large-scale modes are smaller on larger scales. In general, if the relation between halo and matter density is non-linear, the bias estimated from a density field smoothed at any particular scale will be non-linear and will exhibit some scatter (Dekel & Lahav 1998). In our simulation, differences in the bias between different regions of the computational volume seen in Fig. 5 are caused by different numbers and formation histories of clusters and groups in these regions. The regions that exhibit weaker bias (i.e., stronger anti-bias) are the regions that contain clusters with earlier formation epochs. The Coma-size cluster that already had mass of $\approx 1.3 \times 10^{13} h^{-1} M_\odot$ at $z = 3$ exhibits the highest matter overdensity and the strongest anti-bias.

Clusters and groups of galaxies contribute a significant fraction of the galaxy clustering signal at small,

⁴It is clear that dynamical friction *is* important for halo evolution; indeed, binary halo mergers are also due to dynamical friction. However, here we discuss dynamical friction that operates on satellites orbiting inside a more massive system (a group or a cluster), which leads to the decay of their orbits, and, ultimately, to a merger with the central cluster object.

⁵Note that we are bound to use some selection procedure because in most cases we are interested in studying the clustering of a particular (selected) class of objects: halos of a given type, galaxies of a given luminosity or color, etc.

$r \lesssim 1 - 2h^{-1}$ Mpc, scales and significantly affect clustering amplitude at larger scales. The anti-bias arising due to dynamical processes in groups and clusters can therefore explain the anti-bias seen in comparisons of halo and matter two-point correlation functions and power spectra. Our results then imply that understanding of the evolution of small-scale galaxy clustering requires a deeper understanding of the evolution of galaxies in groups and clusters.

The major caveat in interpretation of these dissipationless results is a correspondence between dark matter halos and observable galaxies. We note, however, that the definition of dark matter halo in this study is significantly different from a conventional definition, which eliminates many problems of halo-galaxy mapping related to the overmerging problem (see KGKK and Colín et al. 1998 for discussion). In the framework of the hierarchical structure formation modelled here, it seems likely that in every sufficiently massive ($M \gtrsim 10^{11} h^{-1} M_{\odot}$) *gravitationally bound* halo, at some epoch baryons will cool, form stars, and produce an object resembling a galaxy (e.g., White & Rees 1978; Kauffman, Nusser & Steinmetz 1997; Yepes et al. 1997). This is indeed a cornerstone assumption of the semi-analytical models of galaxy formation (e.g., Somerville & Primack 1998). Therefore, even though we cannot predict detailed properties of galaxies hosted by dark matter halos (which would require inclusion of a substantial amount of additional physics in the simulations), it is likely that the overall halo distribution should be representative of the expected distribution of the overall galaxy population. Excellent agreement between clustering of galaxy-size halos in our simulation and observed galaxy clustering, demonstrated in comparisons of the two-point correlation functions (Colín et al. 1998) and power spectra (see Fig. 3), is an indirect but strong indication in favor of this point.

Anti-bias, similar in amplitude and scale-dependence to that observed in our simulation, has been found in other recent numerical studies that employ either non-adiabatic hydrodynamics (Jenkins et al. 1998b) or semi-analytic recipes (Kauffman et al. 1998ab; Diaferio et al. 1998; Benson et al. 1998) to model galaxy formation and evolution of the two-point correlation function. These studies are very different in their modelling techniques and the agreement indicates that anti-bias is real and is not a numerical artefact of a particular simulation. Anti-bias was traditionally an unfavored proposition because it is easier to envision a biased rather than anti-biased galaxy formation. However, as we have argued above, the anti-bias may arise naturally during the dynamical evolution of the halo population, even though halo formation is biased. Indeed, all of the numerical studies mentioned above are similar to the present study in explicit modelling of the orbital evolution of halos in groups and clusters. Diaferio et al. (1998) present bias profiles $b(r)$ of the clusters in their simulation that are in good qualitative agreement with the profiles shown in Fig. 6, indicating that similar dynamical processes are probably causing the anti-bias in their study.

We can therefore expect that simulations affected by the overmerging problem and in which a recipe for splitting or weighting the overmerged halos is used may overestimate the clustering amplitude at small-scales and not show (or show a weaker) anti-bias. The amount of anti-bias should also depend on the box size because small-size

($\lesssim 30 - 50h^{-1}$ Mpc) boxes are unlikely to contain clusters in the high-mass tail of the mass function. Such a trend is indeed observed; the comparison of bias in the Λ CDM simulations of $30h^{-1}$ Mpc and $60h^{-1}$ Mpc boxes presented in KGKK and Colín et al. (1998) shows that anti-bias is stronger in the $60h^{-1}$ Mpc simulation. Finally and most importantly, the sensitivity of the small-scale bias amplitude to the abundance and evolution histories of clusters indicates that we can expect some differences between cosmological models. The models that form clusters at systematically later epochs and/or in lesser abundance, should exhibit a weaker anti-bias (or even absence of anti-bias), than models that form clusters earlier and in larger numbers. Thus, for example, a τ CDM model appears to result in a higher value of $z = 0$ bias than the Λ CDM model (Kauffman et al. 1998ab, Colín et al. 1998; Diaferio et al. 1998). A more systematic large-box study is needed, however, to test and quantify such dependence on cosmology.

We would like to note that the anti-bias (in the amount predicted by the numerical studies) is actually needed to reconcile the otherwise very successful Λ CDM model with observed galaxy clustering at $z = 0$ (e.g., Klypin, Primack & Holtzman 1996; Cole et al. 1997; Jenkins et al. 1998a). Note that this requirement applies to the overall galaxy population represented in large galaxy surveys such as the CfA and APM; sub-populations of galaxies may exhibit significantly different clustering properties, as is indicated by the differences between clustering of spiral and elliptical galaxies (e.g. Guzzo et al. 1997), infrared- and optically-selected galaxies (e.g. Hoyle et al. 1998), etc. In the simulation presented here, certain sub-samples of halos are clustered more strongly than the overall population. For example, as shown in Gottlöber, Klypin & Kravtsov (1998), the population of halos that loose mass at $z < 1$ (the halos that are accreted and being tidally stripped by clusters) are actually biased at $z = 0$ with respect to the matter distribution, as opposed to the strongly anti-biased distribution of the entire halo population. The simulation used in our analysis was also used by Kolatt et al. (1998), who showed that interpretation of the high clustering amplitude of the high-redshift galaxies is not unique. The amplitude can be reproduced equally well when these galaxies are assumed to be located in high-mass halos, or are assumed to have smaller masses but undergo a starburst due to a collision/merger with another galaxy. Recent studies by Blanton et al. (1998), Cen & Ostriker (1998), Kauffmann et al. (1998ab), and Diaferio et al. (1998) demonstrate the existence of age, luminosity, color segregation of clustering in their models. Some differences in clustering properties of certain sub-samples from the overall population can therefore be expected.

Another observational requirement for the Λ CDM model is a scale-dependent bias (e.g., Jenkins et al. 1998a): the shape of the observed galaxy correlation function is rather different from the shape of the non-linear matter correlation function; this scale-dependency is also reproduced nicely in the simulations. Recent studies of galaxy power spectrum by Gaztañaga & Baugh (1998) and Hoyle et al. (1998) stress that the anti-bias is required at rather low wavenumbers. However, as we have noted above (see §1) and have illustrated in Fig. 3, the amount of small-scale anti-bias observed in the galaxy-correlation function

(Colín et al. 1998) is sufficient to produce the required anti-bias in the power spectrum at low wavenumbers. Indeed, the power spectrum of the halo distribution in our simulation matches nicely the power spectrum of the APM galaxies at all probed wavenumbers. The matter power spectrum, on the other hand, is different from the galaxy power spectrum at a very high ($> 5 - 10\sigma$) significance level. The existence of non-linear and scale-dependent bias of the galaxy distribution may affect other analyses that either assume there is no bias or that the bias is linear. These include estimates of the matter density Ω from peculiar velocities and redshift distortions (Dekel & Lahav 1998; Pen 1998) and from the observed mass to light ratios in galaxy groups and clusters (Diaferio et al. 1998), estimates of the baryon density in the Universe (e.g., Goldberg & Strauss 1998; Meiksin, White & Peacock 1998), estimates of the cosmological parameters based on the joint analysis of galaxy redshift surveys, cosmic microwave background anisotropies, and high-redshift supernovae (e.g. Eisenstein, Hu & Tegmark & 1998), etc. In this respect, the lesson of the present analysis is that any use of the galaxy density field as a cosmological probe requires very careful testing and evaluation.

7. CONCLUSIONS

We presented results from a study of the origin and evolution of bias of the dark matter halo distribution in a large, high-resolution simulation using a low-matter density, flat, CDM model with cosmological constant. The following conclusions can be drawn from the results presented in this paper.

1. The evolution of the power spectrum of the halo distribution is significantly slower than the evolution of the matter power spectrum at all (both linear and non-linear) scales. The halo and matter power spectra also have significantly different shapes. The differences in shape and rate of evolution imply time- and scale-dependent bias of the halo distribution which is in qualitative agreement with the results of the correlation function analyses. We stress, however that the scale dependence of the bias determined from the power spectrum $b_P(k) \equiv \sqrt{P_h(k)/P_m(k)}$ is different from the scale dependence of $b_\xi(r) \equiv \sqrt{\xi_h(r)/\xi_m(r)}$, because the two statistics are related via the Fourier transform (see §1). Put simply, $b_P(k)$ cannot be obtained from $b_\xi(r)$ by a naive substitution of variable $r \propto 1/k$. At $z = 0$ the halo power spectrum in our simulation matches the observed power spectrum of the APM galaxies well.

2. Despite the differences in shape, the power spectra of both matter and halos exhibit a distinct “inflection point” at approximately the same wavenumber, corresponding to the scale of non-linearity (i.e., the scale at which the power spectra begin to deviate significantly from the linear power spectrum). The inflection scale is $\approx 0.15 - 0.2h$ Mpc $^{-1}$ and coincides with the inflection observed in the power spectrum of APM galaxies (Gaztañaga & Baugh 1998); therefore, we interpret the inflection in the APM power spectrum as the present-day scale of non-linearity k_{NL} . In the simulation analyzed here, k_{NL} evolves with time from $\sim 1h$ Mpc $^{-1}$ at $z = 5$ to $\approx 0.15 - 0.2h$ Mpc $^{-1}$ at $z = 0$. We should note that the distinct inflection point can be seen only in the *real-space* power spectrum; the non-linear amplitude of the redshift-space power spectrum is strongly

suppressed and the inflection in the power spectrum of both matter and halos is smoothed out (see Figs. 3 & 4 in Gottlöber et al. 1998).

3. The analytic fitting formula of Peacock & Dodds (1996), with only minor tuning, provides an excellent match to both the shape and evolution rate of the matter power spectrum in our simulation. The latter probes deep into the non-linear regime, down to wavenumbers of $\sim 200h$ Mpc $^{-1}$ (at $z = 0$); we find that clustering of dark matter in the highly non-linear regime in the simulation is approximately stationary (stable clustering).

4. In addition to b_P , we examine the evolution of bias defined using smoothed halo and matter overdensities (δ_h and δ_m) as $b_\delta \equiv \delta_h/\delta_m$. In agreement with results from the correlation function and power spectrum analyses, we find that b_δ is non-linear (i.e., depends on δ_m) and time-dependent. If we modify the model and assume that halos can retain their identity for a finite period of time after their formation and distinguish between formation and observation epochs z_f and z , the analytic model of Mo & White (1996) can describe both the non-linearity and evolution of b_δ at linear and quasi-linear overdensities ($\delta_m \lesssim 5-7$, here and below the overdensities are smoothed with the top-hat smoothing radius of $5h^{-1}$ Mpc). The original model ($z = z_f$) significantly underestimates the bias of galaxy-size halos at $\delta_m \gtrsim 1$.

5. We argue that at non-linear overdensities the bias evolution is significantly affected by dynamical friction and tidal stripping of halos in groups and clusters. Both processes tend to reduce the number density of cluster halos of a given mass range, thereby reducing the bias and resulting in anti-bias at $z \lesssim 0.5$ at $\delta_m \gtrsim 5$ in the Λ CDM model studied here. The effect of dynamical friction depends sensitively on the cluster formation history, which introduces a certain degree of scatter into the bias b_δ .

In summary, the evolution of the bias of galaxy-size halos observed in the simulation in linear and quasi-linear regimes can probably be fully described using the extended Press-Schechter theory. In other words, the evolution of bias in this regime results from an interplay between halo formation and merging rates in different regions and in the field. In the non-linear regime, the halo bias evolution appears to be driven by the dynamical processes inside clusters and groups. Thus, despite the apparent complexity, we believe that the origin and evolution of bias can be understood in terms of the processes that drive the formation and evolution of dark matter halos and galaxies that they host: collapse from the density peaks, merging, tidal stripping and morphological transformation in the high-density regions. Our results show that *these processes may conspire to produce a halo distribution quite different from the overall distribution of matter*, yet remarkably similar to the observed distribution of galaxies. This result implies that detailed modeling of the small-scale galaxy clustering requires a good understanding of galaxy evolution in clusters. We would like to emphasize, therefore, the importance of further efforts in modeling galaxy evolution in both clusters and in the field.

This work was funded by NSF grant AST-9319970, NASA grant NAG-5-3842, and NATO grant CRG 972148 to the NMSU. We would like to thank Stefan Gottlöber

for many useful discussions. We are grateful to Vladimir Avila-Reese and Claudio Firmani for providing us the Monte-Carlo mass aggregation histories in electronic form, and to Michael Gross whose routine we have used to calculate the age of the Universe. The simulation presented in

this paper was done at the National Center for Supercomputing Applications (NCSA, Urbana-Champaign, Illinois) and on the Origin2000 computer at the Naval Research Laboratory.

REFERENCES

- Adelberger, K.L., Steidel, C.C., Giavalisco, M., Dickinson, M., Pettini, M., Kellogg, M. 1998, ApJ, 505, 18
- Avila-Reese, V., & Firmani, C. 1997, in ASP Conf. Ser. 117, Dark and Visible Matter in Galaxies and Cosmological Implications, ed. M. Persic & P. Salucci (San Francisco: ASP), 416
- Babul, A., & White, S.D.M. 1991, MNRAS, 253, L31
- Bagla, J.S. 1998, MNRAS, 299, 417
- Baugh, C.M., & Efstathiou, G. 1993, MNRAS, 265, 145
- Baugh, C.M., Benson, A.J., Cole, S., Frenk, C.S., Lacey, C.G. 1998, MNRAS, submitted (astro-ph/9811222)
- Bardeen, J., Bond, J.R., Kaiser, N., Szalay, A. 1986, ApJ, 304, 15
- Benson, A.J., Cole, S., Frenk, C.S., Baugh, C.M., Lacey, C.G. 1998, to appear in Proceedings of the Xth Rencontres de Blois (astro-ph/9809171)
- Binney, J., & Tremain, S. 1987, *Galactic Dynamics* (Princeton: Princeton University Press)
- Blanton, M., Cen, R., Ostriker, J.P., Strauss, M.A. 1998, ApJ, submitted (astro-ph/9807029)
- Bond, J.R., Cole, S., Efstathiou, G., & Kaiser, N., 1991, ApJ, 379, 440
- Bower, R.G. 1991, MNRAS, 248, 332
- Brainerd, T.G., & Villumsen, J.V. 1994, ApJ, 431, 477
- Bullock, J.S., Kolatt, T.S., Sigad, Y., Kravtsov, A.V., Klypin, A.A., Primack, J.R., Dekel, A., 1998, in preparation
- Bunn, E.F., & White, M. 1997, ApJ, 480, 6
- Carlberg, R.G., Cowie, L.L., Songaila, A., & Hu, E.M. 1997, ApJ, 484, 538
- Carlberg, R.G., et al. 1998, in "Large Scale Structure in the Universe", Proceedings of the Royal Society Discussion Meeting (astro-ph/9805131)
- Catelan, P., Lucchin, F., Matarrese, S., & Porciani, C. 1998a, MNRAS, 297, 692
- Catelan, P., Matarrese, S., Porciani, C. 1998b, ApJL, 502, 1
- Cen, R., & Ostriker, J.P. 1998, ApJ, submitted (astro-ph/9809370)
- Cole, S., & Kaiser, N. 1989, MNRAS, 237, 1127
- Cole, S., Weinberg, D.H., Frenk, C.S., & Ratra, B. 1997, MNRAS, 289, 37
- Coles, P. 1993, MNRAS, 262, 1065
- Colín, P., Klypin, A.A., Kravtsov, A.V., Khokhlov, A.M. 1998, ApJ, submitted (astro-ph/9809202)
- Connolly, A.J., Szalay, A.S., Brunner, R.J. 1998, ApJ, in press (astro-ph/9803047)
- Croft, R.A.C., Weinberg, D.H., Pettini, M., Hernquist, L., Katz, N. 1998, ApJ, submitted (astro-ph/9809401)
- Davis, M., Efstathiou, G., Frenk, C.S., & White, S.D.M. 1985, ApJ, 292, 371
- Dekel, A., & Silk, J. 1986, ApJ, 303, 39
- Dekel, A., & Lahav, O. 1998, ApJ, submitted (astro-ph/9806193)
- Diaferio, A., Kauffmann, G., Colberg, J.M., White, S.D.M. 1998, MNRAS, submitted (astro-ph/9812009)
- Eisenstein, D.J., Hu, W., & Tegmark, M. 1998, ApJ, 504, L57
- Eke, V.R., Cole, S., & Frenk, C.S. 1996, MNRAS, 282, 263
- Eke, V.R., Navarro, J.F., Frenk, C.S. 1998, ApJ, 503, 569
- Evrard, A.E. 1997, ApJ, 292, 289
- Falco, E.E., Shapiro, I.I., Moustakas, L.A., Davis, M. 1997, ApJ, 484, 70
- Fry, J.N. 1996, ApJ, 461, L65
- Fry, J.N., & Gaztañaga, E. 1993, MNRAS, 413, 447
- Jenkins, A. et al. 1998a, ApJ, 499, 20
- Jenkins, A. et al. 1998b, poster presented at the Conference "Evolution of LSS: from Recombination to Garching" (Garching, Germany, August 1998)
- Jing, Y.P. 1998, ApJ, 503, L9
- Gaztañaga, E., & Baugh, C.M. 1998, MNRAS, 294, 229
- Giavalisco, M., Steidel, C.C., Adelberger, K.L., Dickinson, M.E., Pettini, M., Kellogg, M. 1998, ApJ, 503, 543
- Goldberg, D.M., & Strauss, M.A. 1998, ApJ, 495, 29
- Gottlöber, S., Klypin, A.A., & Kravtsov, A.V. 1998, (astro-ph/9810445)
- Guzzo, L., Strauss, M.A., Fisher, K.B., Giovanelli, R., & Haynes, M.P. 1997, ApJ, 489, 37
- Hockney, R.W., & Eastwood, J.W. 1981, *Computer simulations using particles* (New York: McGraw-Hill)
- Hoyle, F., Baugh, C.M., Shanks, T., Ratcliffe, A. 1998, MNRAS, submitted (astro-ph/9812137)
- Kaiser, N. 1984, ApJ, 284, L9
- Katz, N., Hernquist, L., & Weinberg, D.H. 1998, ApJ, submitted (astro-ph/9806257)
- Kauffmann, G., Nusser, A., & Steinmetz, M. 1997, MNRAS, 286, 795
- Kauffmann, G., Colberg, J.M., Diaferio, A., White, S.D.M. 1998a, MNRAS, submitted (astro-ph/9805283)
- Kauffmann, G., Colberg, J.M., Diaferio, A., White, S.D.M. 1998b, MNRAS, submitted (astro-ph/9809168)
- Kitayama, T., & Suto, Y. 1996, MNRAS, 280, 638
- Klypin, A.A., Primack, J.R., & Holtzman, J. 1996, ApJ, 466, 13
- Klypin, A.A., & Holtzman, J. 1997, preprint astro-ph/9712217 (see also <http://astro.nmsu.edu/~aklypin/pmcode.html>)
- Klypin, A.A., Gottlöber, S., Kravtsov, A.V., & Khokhlov, A.M. 1999, ApJ, in press (astro-ph/9708191) (KGKK)
- Kolatt, T.S., Bullock, J.S., Somerville, R., Sigad, Y., Jonsson, P., Kravtsov, A.V., Klypin, A.A., Primack, J.R., Dekel, A. 1998, Nature, submitted
- Kravtsov, A.V., Klypin, A.A., & Khokhlov, A.M. 1997, ApJS 111, 73
- Lacey, C., & Cole, S. 1993, MNRAS, 262, 627
- Lacey, C., & Cole, S. 1994, MNRAS, 271, 676
- Lahav, O., Rees, M.J., Lilje, P.B., Primack, J.R. 1991, MNRAS, 253, 17
- Le Fèvre, O., Hudon, D., Lilly, S.J., Crampton, D., Hammer, F., & Tresse, L. 1996, ApJ, 461, 534
- Ma, C.-P. 1999, ApJ, in press (astro-ph/9808130)
- Madore, B.F. et al. 1998, ApJ, in press (astro-ph/9812157)
- Mann, R.G., Peacock, J.A., & Heavens, 1998 MNRAS, 293, 209
- Meiksin, A., White, M., & Peacock, J.A. 1998, MNRAS, in press (astro-ph/9812214)
- Mo, H.J., & White, S.D.M. 1996, MNRAS, 282, 347
- Mo, H.J., Jing, Y.P., & White, S.D.M. 1996, MNRAS, 282, 1096
- Moscardini, L., Coles, P., Lucchin, F., Matarrese, S. 1998, MNRAS, 299, 95
- Narayanan, V.K., Berlind, A., Weinberg, D.H. 1998, ApJ, submitted (astro-ph/9812002)
- Navarro, J.F., Frenk, C.S., White, S.D.M. 1996, ApJ, 462, 563
- Navarro, J.F., Frenk, C.S., White, S.D.M. 1997, ApJ, 490, 493 (NFW)
- Peacock, J.A. 1997, MNRAS, 284, 885
- Peacock, J.A., & Dodds, S.J. 1996, MNRAS, 280, L19 (PD96)
- Peebles, P.J.E. 1980, *The Large-Scale Structure of the Universe* (Princeton: Princeton Univ. Press)
- Pen, U.-L. 1998, ApJ, 504, 601
- Perlmutter, S., et al. 1998, ApJ, in press (astro-ph/9812133)
- Porciani, C., Matarrese, S., Lucchin, F., Catelan, P. 1998a, MNRAS, submitted (astro-ph/9801290)
- Porciani, C., Catelan, P., & Lacey, C. 1998b, ApJL, submitted (astro-ph/9811477)
- Postman, M., Lauer, T.R., Szapudi, I., & Oegerle, W. 1998, ApJ, 506, 33
- Press W.H., & Schechter, P. 1974, ApJ, 187, 425
- Roukema, B.F., Peterson, B.A., Quinn, P.J., & Rocca-Volmerange 1997, MNRAS, 292, 835
- Salaris, M., & Cassisi, S. 1998, MNRAS, 298, 166
- Scherrer, R.J., & Weinberg, D.H. 1998, ApJ, 504, 607
- Shepherd, C.W., Carlberg, R.G., Yee, H.K.C., & Ellingson, E. 1997, ApJ, 479, 82
- Sheth, R.K., & Lemson, G. 1998, MNRAS, submitted (astro-ph/9808138)
- Smith, C.C., Klypin, A., Gross, M.A.K., Primack, J.R., & Holtzman, J. 1998, MNRAS, 297, 910
- Somerville, R., & Primack, J.R. 1998, MNRAS, in press (astro-ph/9802268)
- Steidel, C.C., Adelberger, K.L., Dickinson, M., Giavalisco, M., Pettini, M., & Kellogg, M. 1998, ApJ, 492, 428
- Tadros, H., & Efstathiou, G. 1996, MNRAS, 282, 1381
- Taruya, A., Koyama, K., & Soda, J. 1998, ApJ, in press (astro-ph/9807005)
- Taruya, A., & Soda, J. 1998, ApJ, submitted (astro-ph/9809204)
- Tegmark, M., & Peebles, P.J.E. 1998, ApJ, 500, L79
- Tegmark, M., & Bromley, B.C. 1998, ApJ, submitted (astro-ph/9809324)

Tegmark, M., Hamilton, A.J.S., Strauss, M.A., Vogeley, M.S., & Szalay, A. 1998, ApJ, 499, 555
Weinberg, D.H., Croft, R.A.C., Hernquist, L., Pettini, M. 1998, ApJ, submitted ([astro-ph/9810011](#))

White, S.D.M., & Rees, M. 1978, MNRAS, 183, 341
Yepes, G., Kates, R., Khokhlov, A., & Klypin, A. 1997, MNRAS, 284, 235